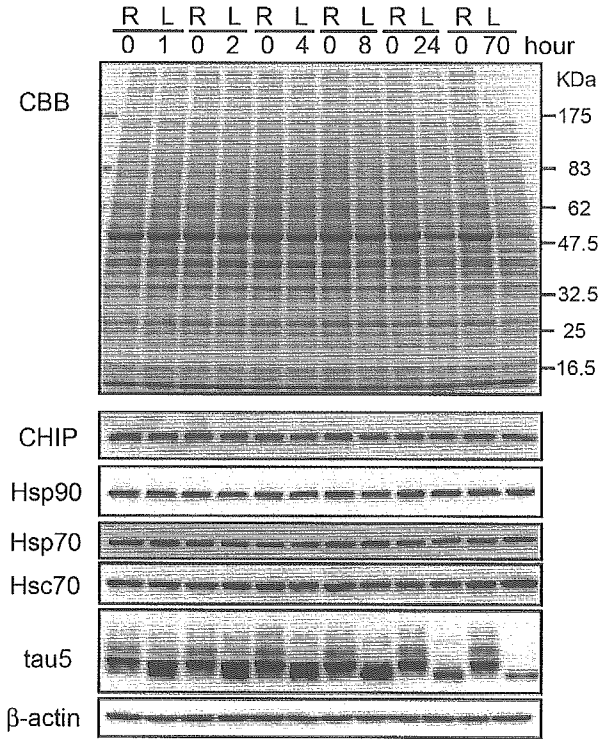

Fig. 3 Effect of post-mortem interval on protein degradation in mouse brains. TBS-soluble fractions from mouse hemibrains were separated by SDS–PAGE then immunoblotted using CHIP, Hsp90, Hsp70, Hsc70, tau5 and β-actin antibodies. One hemibrain (R) was quickly frozen and stored at – 80°C (post-mortem interval zero). The other (L) was kept at room temperature for 1, 2, 4, 8, 24 or 70 h after death. Equal volumes of samples derived from 0.33 mg wet-weight tissue were resolved by SDS–PAGE. Upper panel shows Coomassie Brilliant Blue (CBB) staining with molecular weight markers.

CHIP in JNPL3 mouse brain was similar to that in wild type (compare Fig. 4b with Fig. 4a). The level of CHIP in spinal cord was only 20% of that in cerebellum. The level of sarkosyl-insoluble tau was inversely related to CHIP levels in cerebellum and spinal cord. Because amounts of sarkosyl-insoluble tau were inversely related to the amount of CHIP in AD brains, we checked the CHIP levels in both cerebellum and spinal cord regions. CHIP levels were more than 15% higher in JNPL3 mouse cerebellar regions than those in non-Tg mouse cerebellar regions, but no difference was found in the levels in the spinal cords of JNPL3 and non-Tg mice when protein levels were normalized with respect to β-actin (cerebellum, $p = 0.023$; spinal cord, $p = 0.49$) (Fig. 4c). Neuronal loss in the spinal cord of JNPL3 mice (Lewis *et al.* 2000) was confirmed by checking the protein levels of NSE as a marker. As shown in Fig. 4(e), the NSE level was significantly lower in JNPL3 mouse spinal cord ($p = 0.0035$). When CHIP levels were normalized with respect to NSE, the levels in JNPL3 mouse spinal cords were higher than those in non-Tg mouse spinal cords but the difference was not significant different ($p = 0.10$) (Fig. 4d).

As the development of tau pathology in the JNPL3 mouse is age dependent, we checked the levels of both CHIP and Hsp90 at different ages. By 11 months of age, the CHIP level in spinal cord was slightly increased but the Hsp90 level was not (Fig. 5a). In cerebellum, no significant differences in either CHIP or Hsp90 levels were found during ageing (Fig. 5b). Although 64-kDa tau was detected in JNPL3 mouse cerebellum, the accumulation of sarkosyl-insoluble tau in spinal cord was greater than that in cerebellum. These data suggest that overexpression of P301L tau increases the amount of CHIP which then attenuates NFT formation, although sufficient levels of CHIP are not produced in spinal cord.

Increased level of insoluble tau in aged *CHIP–/–* mouse brain

Unlike the CHIP-deficient mice described by Dai *et al.* (2003), our *CHIP–/–* mice showed significant anatomical abnormalities such as lower bodyweight and dysbasia. Some 95% of *CHIP–/–* mice die by the third week after birth. The remaining mice survive for more than 1 year. These phenotypes might be due to their genetic backgrounds because our heterozygous mice were maintained on a C57BL/6 strain and back-crossed over five times (Murata S. *et al.*, unpublished observation). We first analyzed the involvement of CHIP in tau phosphorylation and degradation using 2.5- and 18-month-old mouse brains. There were no significant differences in the amounts of soluble tau or tau phosphorylation between wild-type and CHIP-deficient mice (Fig. 6a). We analyzed the solubility of tau protein by extracting brains using buffers with increasing extraction strengths to determine whether tau becomes insoluble in CHIP-deficient mice. Interestingly, both aged *CHIP–/–* and heterozygous (*CHIP+/–*) mouse brains showed increased levels of SDS-insoluble tau, detected by both phosphorylation-independent and -dependent tau antibodies (Fig. 6a). Three additional 18-month-old *CHIP–/–*, *CHIP+/–* and *CHIP+/+* mouse brains were analyzed for insoluble tau accumulation. Although the amount of SDS-insoluble tau varied, it tended to increase with greater CHIP deficiency (Fig. 6c). When we quantified the protein levels of CHIP, heterozygous mouse brains had only 6% of that found in wild-type mouse brains (Fig. 6b). These data suggest that suppression of CHIP induces abnormal tau accumulation in a phosphorylation-independent manner in aged mice.

Discussion

Previous studies have linked CHIP with tau ubiquitination and degradation (Hatakeyama *et al.* 2004; Petrucelli *et al.* 2004; Shimura *et al.* 2004). In this report, we describe the biochemical features of CHIP in human and mouse brain. An

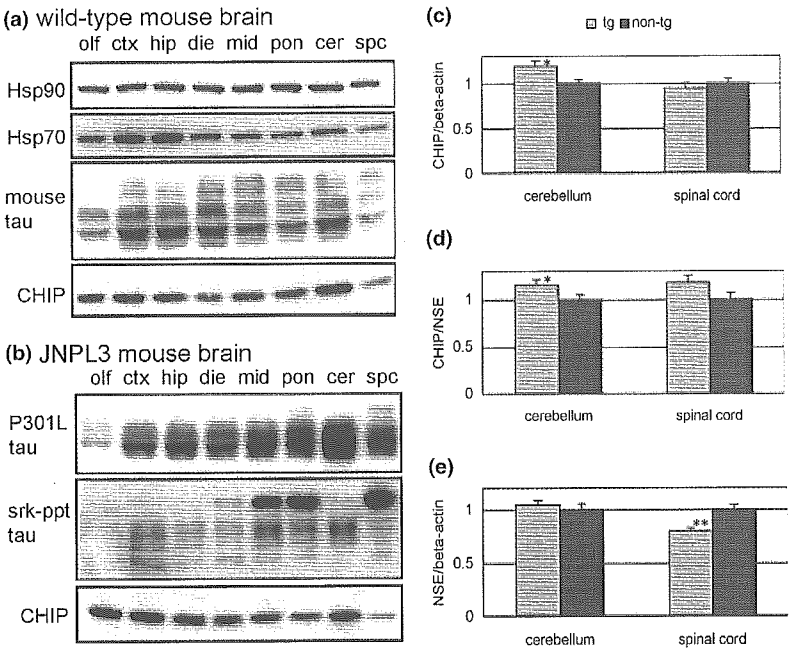

Fig. 4 CHIP distribution in wild-type and JNPL3 mouse brain. (a) TBS-soluble fractions prepared from olfactory bulb (olf), cerebral cortex (ctx), hippocampus (hip), diencephalons (die), midbrain (mid), pons and medulla oblongata (pon), cerebellum (cer) and spinal cord (spc) of 9.3-month-old female mouse were immunoblotted using Hsp90, Hsp70, tau5 and CHIP (R1) antibodies. Equal volumes of samples based on wet weight was resolved by SDS–PAGE. (b) TBS-soluble fractions prepared from the same regions of 9.3-month-old female JNPL3 mouse were blotted using E1 and CHIP (R1) antibodies (top and bottom panel respectively). Sarkosyl-insoluble fractions (srk-ppt) derived from 5 mg wet-weight of each brain region was blotted using E1 antibody (middle). Amounts of CHIP normalized with respect to β-actin (c) and NSE (d), and NSE normalized with respect to β-actin, in cerebellum and spinal cord from Tg (4–10-month-old females, $n = 8$) and non-Tg littermates (females, $n = 8$). Values are mean ± SEM. $^{*}p < 0.05$, $^{**}p < 0.01$ versus non-Tg (unpaired *t*-test with Welch correlation).

increased level of CHIP in AD brain, with respect to controls, was observed. When we analyzed individual differences, the protein levels of CHIP corresponded with Hsp90 levels. An inverse relationship between tau aggregation and CHIP levels was observed in humans and in our mice with tauopathy. We found that a lack of CHIP influenced insoluble tau accumulation. These data suggest that CHIP may protect against tau aggregation and NFT formation.

CHIP is a ubiquitin protein ligase that selectively ubiquitinates denatured proteins when the substrate is captured by a molecular chaperone, including Hsp90 or Hsc70 (Murata *et al.* 2001). Involvement of Hsc70 in the CHIP-dependent ubiquitination of CFTR was also reported (Meacham *et al.* 2001). Connell *et al.* (2001) noted that the ubiquitination-dependent instability of the Hsp90-trapped glucocorticoid receptor was promoted by CHIP. Dai *et al.* (2003) reported that CHIP regulates the activation of Hsp70 by inducing trimerization and transcriptional activation of heat shock factor 1 (HSF-1). Petrucelli *et al.* (2004) found that Hsp70 could reduce tau levels in both a cell culture system and mouse brain. We present novel evidence that levels of Hsp90 correspond to CHIP levels in aged human brains. As Hsp90 often pairs with Hsc/Hsp70, the two chaperones are often thought to be part of a single multichaperone machine (for review, see Young *et al.* 2001), but accumulating evidence suggests that both also work alone. In addition to our CHIP/Hsp90 response, up-regulation of Hsp70 in AD brains has also been reported (Yoo *et al.* 1999). This suggests that in the human brain CHIP might modulate this machinery by interacting directly, and specifically, with either protein in response to the nature of protein misfolding and aggregation.

Immunohistochemical studies found CHIP co-localized with tau-positive lesions in neurons and glia (Petrucelli *et al.* 2004). The number of CHIP-immunoreactive lesions was 50–70% for Pick's disease, 5–10% for AD and 1–5% for both progressive supranuclear palsy and corticobasal degeneration in these studies when CHIP was confirmed using a CHIP-specific antibody with peptide pre-absorption. In contrast, we reported that anti-CHIP antibody stained NFT-bearing cells in progressive supranuclear palsy brain, but only faintly in AD (Hatakeyama *et al.* 2004). This discrepancy might be due to the different specificities of the antibodies. We produced CHIP antibodies from recombinant proteins and confirmed their specificity by western blotting (Fig. 1). Our biochemical observation showed that the amounts of sarkosyl-insoluble tau did not correspond to

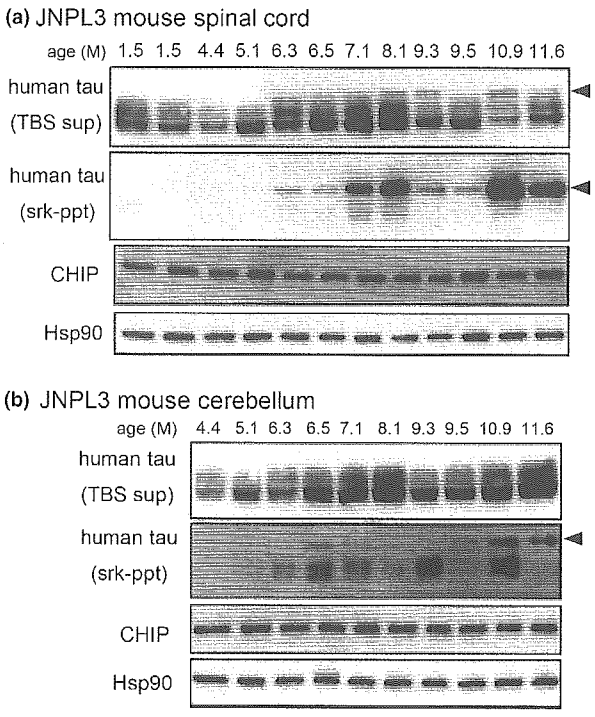

Fig. 5 Changes in CHIP and Hsp90 levels in JNPL3 mouse spinal cord and cerebellum with age. (a) Samples from spinal cords of 1.5–11.6-month (M)-old female JNPL3 mice were analyzed. TBS-soluble fractions (TBS sup) were immunoblotted using E1, CHIP and Hsp90 antibodies. The second panel from the top shows sarkosyl-insoluble fractions (srk-ppt) blotted with E1 antibody (note that the exposure time was shorter than that used for middle panel of Fig. 4b). Equal volumes, based on wet weight, of each sample were resolved by SDS–PAGE. The 64-kDa band (arrowhead) was detected by the E1 antibody in both TBS sup and srk-ppt. (b) Samples from cerebellum of 4.4–11.6-month-old female JNPL3 mice. TBS-soluble fractions (TBS sup) were immunoblotted using E1, CHIP and Hsp90 antibodies. The second panel from the top shows sarkosyl-insoluble fractions (srk-ppt) blotted with E1 antibody (note that the exposure time was much longer than for second panel from top in Fig. 5a).

CHIP levels in NFT-enriched fractions (Fig. 2a). If a direct association between CHIP and Hsp90 can be confirmed, the previous report showing an inverse relationship between aggregated tau and the level of Hsp90 in tau Tg mice and AD brains (Dou *et al.* 2003) will support our observations. The reduction in the levels of CHIP/Hsp90 may stem from the degradation of these proteins together with maturing tau aggregation by a lysosomal pathway or other mechanism. Although more precise experiments are required to confirm the sequestration of CHIP with tau inclusions, we suspect that CHIP expression is up-regulated to cooperate with molecular chaperones for suppression of NFT formation at the early stage of AD.

Here, we quantified CHIP levels in JNPL3 mouse brains in which P301L tau is overexpressed. We observed increased levels of CHIP in the cerebellar regions of JNPL3 mice when compared with age-matched non-Tg littermates and that cerebellar regions of JNPL3 mice had less sarkosyl-insoluble tau than spinal cords, whereas the total tau levels in cerebellum were higher than those in spinal cords (Fig. 4). The finding that the cerebellum had less sarkosyl-insoluble tau than the spinal cord does not contradict the original observations of the pathological features in JNPL3 mouse brain (Lewis *et al.* 2001). We observed that age-dependent hyperphosphorylated tau accumulation in cerebellum of JNPL3 mice was delayed (Fig. 5). In AD, NFTs are observed in the hippocampus and neocortex but not the cerebellum (Larner 1997). Previously, we reported that hyperphosphorylation of tau after changes in glucose metabolism was lower in the cerebellum than in the hippocampus and cerebral cortex (Planel *et al.* 2004). Both CHIP expression and resistance of tau hyperphosphorylation may attenuate abnormal tau accumulation in mouse cerebellum. Because an inverse accumulation of sarkosyl-insoluble tau with CHIP levels, but not Hsp levels, was observed in the mouse brain, CHIP might be essential in preventing prevent tau aggregation whereas Hsp90 and Hsp70 have additional functions in many cellular processes, including protein folding, transport, degradation and signal transduction. The inconsistency between humans and mice might be explained by brain regional differences. To determine whether Hsp90 cooperates with CHIP to prevent tau aggregation in mouse brain, a model that develops tau pathology in cerebral cortex such as the human P301S tau Tg mouse would be more useful (Allen *et al.* 2002). In contrast to human AD brains, which showed massive accumulation of PHF-tau and reduced levels of CHIP, we found no reduction in CHIP levels in either cerebellum or spinal cord of aged JNPL3 mice. It is possible that unknown ubiquitin ligases other than CHIP might be reduced in these brain regions. Further studies are necessary to determine what other factors might be responsible for tau aggregation in JNPL3 mice.

The biochemical analysis of tau in the *CHIP* knockout mouse brains revealed a slight increase in detergent-insoluble tau with no change in the total amount of tau. This indicates that, although eliminating CHIP is not sufficient to induce NFT formation, a lack of CHIP is involved is NFT formation when tau abnormalities are present. As the precise roles of the chaperone system and the ubiquitin proteasomal system within the pathogenesis of tauopathies have yet to be determined, cross-breeding the *CHIP* knockout mouse with a tau Tg mouse may be beneficial.

To our knowledge, this is the first *in vivo* study of CHIP's properties. We confirmed that co-chaperone CHIP was up-regulated by early NFT formation and prevented tau aggregation with the help of molecular chaperones in human and mouse brains. Therefore, CHIP can modify the disease states of human tauopathies when working in combination with its molecular chaperones.

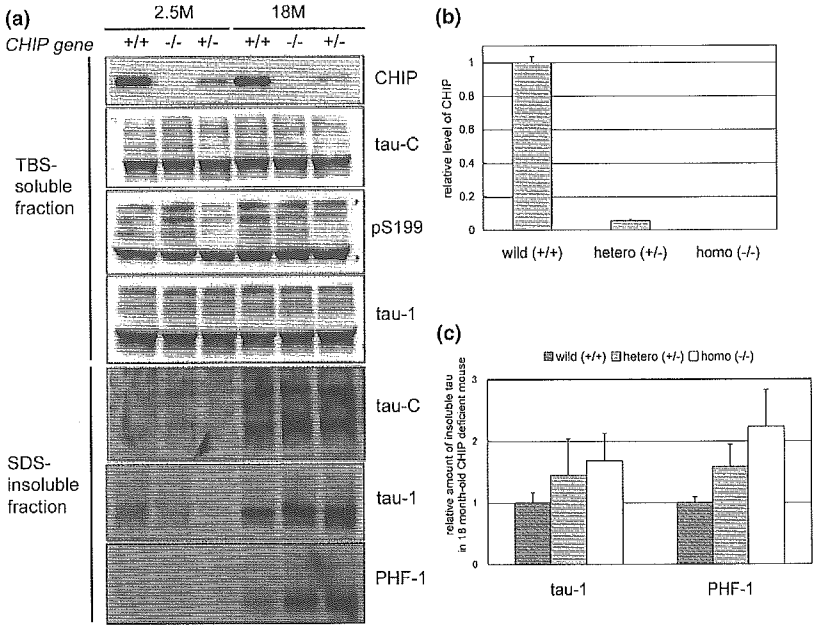

Fig. 6 Insoluble tau accumulation in *CHIP* knockout mouse brain. (a) TBS-soluble fractions derived from 2.5- and 18-month (M)-old *CHIP*+/+, *CHIP*+/– and *CHIP*–/– mouse brains were immunoblotted using CHIP (R1), tauC, pS199 and tau-1 antibodies. SDS-insoluble fractions extracted with 70% formic acid were immunoblotted using tauC, tau1 and PHF-1 antibodies. Samples containing equal amounts of protein were resolved by SDS–PAGE. (b) Relative levels of CHIP in 18-month-old mouse brains ($n = 3$). Values are mean ± SEM with respect to levels in wild-type mice. (c) Amounts of insoluble tau in 18-month-old mouse brains ($n = 3$). SDS-insoluble fractions extracted with 70% formic acid were immunoblotted using tau1 and PHF-1 antibodies, then quantified by means of an image analyzer. Values are mean ± SEM with respect to levels in wild-type mice.

Acknowledgements

This work was supported by research grants from RIKEN Brain Science Institute and a Grant-in-Aid for Scientific Research (Japan Ministry of Education, Culture, Sports, Science and Technology). We are grateful to Bonnie Lee La Madeleine for editing this manuscript.

References

Allen B., Ingram E., Takao M. *et al.* (2002) Abundant tau filaments and nonapoptotic neurodegeneration in transgenic mice expressing human P301S tau protein. *J. Neurosci.* **22**, 9340–9351.

Ballinger C. A., Connell P., Wu Y., Hu Z., Thompson L. J., Yin L. Y. and Patterson C. (1999) Identification of CHIP, a novel tetratricopeptide repeat-containing protein that interacts with heat shock proteins and negatively regulates chaperone functions. *Mol. Cell. Biol.* **19**, 4535–4545.

Connell P., Ballinger C. A., Jiang J., Wu Y., Thompson L. J., Hohfeld J. and Patterson C. (2001) The co-chaperon CHIP regulates protein triage decisions mediated by heat-shock proteins. *Nat. Cell Biol.* **3**, 93–96.

Dai Q., Zhang C., Wu Y. *et al.* (2003) CHIP activates HSF1 and confers protection against apoptosis and cellular stress. *EMBO J.* **22**, 5446–5458.

Dickson D. W., Lin W. K., Ksiezak-Reding H. and Yen S.-H. (2000) Neuropathologic and molecular considerations. *Adv. Neurol.* **82**, 9–27.

Dou F., Netzer W. J., Tanemura K., Li F., Hartl F. U., Takashima A., Gouras G. K., Greengard P. and Xu H. (2003) Chaperons increase association of tau protein with microtubules. *Proc. Natl Acad. Sci. USA* **100**, 721–726.

Gong C.-X., Liu F., Grundke-Iqbal I. and Iqbal K. (2005) Post-translational modification of tau protein in Alzheimer's disease. *J. Neural. Transm.* **112**, 813–838.

Grundke-Iqbal I., Iqbal K., Quinlan M., Tung Y. C., Zaidi M. S. and Wisniewski H. M. (1986) Microtubule-associated protein tau: a component of Alzheimer-paired helical filaments. *J. Biol. Chem.* **261**, 6084–6089.

Hatakeyama S., Yada M., Matsumoto M., Ishida N. and Nakayama K. I. (2001) U box proteins as a new family of ubiquitin-protein ligases. *J. Biol. Chem.* **276**, 33111–33120.

Hatakeyama S., Matsumoto M., Kamura T., Murayama M., Chui D.-H., Planel E., Takahashi R., Nakayama K. I. and Takashima A. (2004) U-box protein carboxyl terminus of Hsc70-interacting protein (CHIP) mediates poly-ubiquitylation preferentially on four-repeat tau and is involved in neurodegeneration of tauopathy. *J. Neurochem.* **91**, 299–307.

Imai Y., Soda M., Hatakeyama S., Akagi T., Hashikawa T., Nakayama K. and Takahashi R. (2002) CHIP is associated with Parkin, a gene responsible for familial Parkinson's disease, and enhances its ubiquitin ligase activity. *Mol. Cell* **10**, 55–67.

Ishihara T., Hong M., Zhang B., Nakagawa Y., Lee M. K., Trojanowski J. Q. and Lee V. M.-Y. (1999) Age-dependent emergence and progression of a tauopathy in transgenic mice overexpressing the shortest human tau isoform. *Neuron* **24**, 751–762.

Jiang J., Ballinger C. A., Wu Y., Dai Q., Cyr D. M., Hohfeld J. and Patterson C. (2001) CHIP is a U-box-dependent E3 ubiquitin ligase: identification of Hsc70 as a target for ubiquitylation. *J. Biol. Chem.* **276**, 42938–42944.

Jicha G. A., Berenfeld B. and Davies P. (1999) Sequence requirements for formation of conformational variants of tau similar to those found in Alzheimer's disease. *J. Neurosci. Res.* **55**, 713–723.

Johnson G. V. and Bailey C. D. (2002) Tau, where are we now? *J. Alzheimers Dis.* **4**, 375–398.

Kenessey A., Nacharaju P., Ko L.-W. and Yen S.-H. (1997) Degradation of tau by lysosomal enzyme cathepsin D: implication for Alzheimer neurofibrillary degeneration. *J. Neurochem.* **69**, 2026–2038.

Larner A. J. (1997) The cerebellum in Alzheimer's disease. *Dement. Geriatr. Cogn. Disord.* **8**, 203–209.

Lewis J., McGowan E., Rockwood J. *et al.* (2000) Neurofibrillary tangles, amyotrophy and progressive motor disturbance in mice expressing mutant (P301L) tau protein. *Nat. Genet.* **25**, 402–405.

Lewis J., Baker M., Van Slegtenhorst M. and Hutton M. (2001) Molecular genetics and transgenic modeling of the tauopathies in Alzheimer's disease, in *Advances in Etiology, Pathogenesis and Therapeutics* (Iqbal K., Sisodia S. S., Winblad B., eds), pp. 71–85. Jon Wiley & Sons, Chichester.

Meacham G., Patterson C., Zhang W., Younger J. M. and Cyr D. M. (2001) The Hsc70 co-chaperone CHIP targets immature CFTR for proteasomal degradation. *Nat. Cell Biol.* **3**, 100–105.

Muchowski R. J. and Wacker J. L. (2005) Modulation of neurodegeneration by molecular chaperones. *Nat. Rev.* **6**, 11–22.

Murata S., Minami Y., Minami M., Chiba T. and Tanaka K. (2001) CHIP is a chaperone-dependent E3 ligase that ubiquitylates unfolded protein. *EMBO Report* **2**, 1133–1138.

Petrucelli L., Dickson D., Kehoe K. *et al.* (2004) CHIP and Hsp70 regulate tau ubiquitination, degradation and aggregation. *Hum. Mol. Genet.* **13**, 703–714.

Planel E., Miyasaka T., Launey T., Chui D.-H., Tanemura K., Sato S., Murayama O., Ishiguro K., Tatebayashi Y. and Takashima A. (2004) Alterations in glucose metabolism induce hypothermia leading to tau hyperphosphorylation through differential inhibition of kinase and phosphatase activities: implications for Alzheimer's disease. *J. Neurosci.* **24**, 2401–2411.

Sahara N., Lewis J., DeTure M., McGowan E., Dickson D. W., Hutton M. and Yen S.-H. (2002) Assembly of tau in transgenic animals expressing P301L tau: alteration of phosphorylation and solubility. *J. Neurochem.* **83**, 1498–1508.

Sherman M. Y. and Goldberg A. L. (2001) Cellular defenses against unfolded proteins: a cell biologist thinks about neurodegenerative diseases. *Neuron* **29**, 15–32.

Shimura H., Schwartz D., Gygi S. P. and Kosik K. S. (2004) CHIP–Hsc70 complex ubiquitinates phosphorylated tau and enhances cell survival. *J. Biol. Chem.* **279**, 4869–4876.

Tanemura K., Murayama M., Akagi T., Hashikawa T., Tominaga T., Ichikawa M., Yamaguchi H. and Takashima A. (2002) Neurodegeneration with tau accumulation in a transgenic mouse expressing V337M human tau. *J. Neurosci.* **22**, 133–141.

Urushitani M., Kurisu J., Tateno M., Hatakeyama S., Nakayama K., Kato S. and Takahashi R. (2004) CHIP promotes proteasomal degradation of familial ALS-linked mutant SOD1 by ubiquitinating Hsp/Hsc70. *J. Neurochem.* **90**, 231–244.

Xu W., Marcu M., Yuan X., Mimnaugh E., Patterson C. and Neckers L. (2002) Chaperone-dependent E3 ubiquitin ligase CHIP mediates a degradative pathway for c-ErbB2/Neu. *Proc. Natl Acad. Sci. USA* **99**, 12847–12852.

Yan S.-D., Chen X., Schmidt A.-M. *et al.* (1994) Glycated tau protein in Alzheimer disease: a mechanism for induction of oxidative stress. *Proc. Natl Acad. Sci. USA* **91**, 7787–7791.

Yoo B. C., Seidl R., Cairns N. and Lubec G. (1999) Heat-shock protein 70 levels in brain of patients with Down syndrome and Alzheimer's disease. *J. Neural Transm. Suppl.* **57**, 315–322.

Young J. C., Moarefi I. and Hartl F. U. (2001) Hsp90: a specialized but essential protein-folding tool. *J. Cell Biol.* **154**, 267–273.

International weekly journal of science

nature

A heterodimeric complex that promotes the assembly of mammalian 20S proteasomes

Yuko Hirano[*1], Klavs B. Hendil[*2], Hideki Yashiroda[*1], Shun-ichiro Iemura[*3], Ryoichi Nagane[*3], Yusaku Hioki[*3], Tohru Natsume[*3], Keiji Tanaka[*1] & Shigeo Murata[*1,4]

[*1]*Laboratory of Frontier Science, Core Technology and Research Center, Tokyo Metropolitan Institute of Medical Science, Bunkyo-ku, Tokyo 113-8613, Japan.*
[*2]*Institute of Molecular Biology and Physiology, University of Copenhagen, 13 Universitetsparken, DK 2100 Copenhagen, Denmark.*
[*3]*National Institute of Advanced Industrial Science and Technology, Biological Information Research Center, Kohtoh-ku, Tokyo 135-0064, Japan.*
[*4]*PRESTO, Japan Science and Technology Agency, Kawaguchi, Saitama 332-0012, Japan.*

Reprinted from Nature, Vol. 437, No. 7063, pp. 1381–1385, 27 October 2005

A heterodimeric complex that promotes the assembly of mammalian 20S proteasomes

Yuko Hirano[1], Klavs B. Hendil[2], Hideki Yashiroda[1], Shun-ichiro Iemura[3], Ryoichi Nagane[3], Yusaku Hioki[3], Tohru Natsume[3], Keiji Tanaka[1] & Shigeo Murata[1,4]

The 26S proteasome is a multisubunit protease responsible for regulated proteolysis in eukaryotic cells[1,2]. It comprises one catalytic 20S proteasome and two axially positioned 19S regulatory complexes[3]. The 20S proteasome is composed of 28 subunits arranged in a cylindrical particle as four heteroheptameric rings, $\alpha_{1-7}\beta_{1-7}\beta_{1-7}\alpha_{1-7}$ (refs 4, 5), but the mechanism responsible for the assembly of such a complex structure remains elusive. Here we report two chaperones, designated proteasome assembling chaperone-1 (PAC1) and PAC2, that are involved in the maturation of mammalian 20S proteasomes. PAC1 and PAC2 associate as heterodimers with proteasome precursors and are degraded after formation of the 20S proteasome is completed. Overexpression of PAC1 or PAC2 accelerates the formation of precursor proteasomes, whereas knockdown by short interfering RNA impairs it, resulting in poor maturation of 20S proteasomes. Furthermore, the PAC complex provides a scaffold for α-ring formation and keeps the α-rings competent for the subsequent formation of half-proteasomes. Thus, our results identify a mechanism for the correct assembly of 20S proteasomes.

It is presumed that assembly of 20S proteasomes starts by the spontaneous formation of α-rings[6–8]; however, the exact mechanism responsible for α-ring formation remains elusive. Seven β-subunits, some of which are in precursor forms, are arranged on the α-ring to form a complex named the 'half-proteasome', which consists of one α-ring, one β-ring and the chaperone protein Ump1. To complete maturation of the 20S proteasome, two half-proteasomes dimerize, the propeptides of β-subunits are removed and Ump1 is degraded[9–14]. This model is based mainly on studies in yeast. In mammals, POMP or Proteassemblin, a homologue of yeast Ump1 referred to here as human Ump1 (hUmp1), is also implicated in assembly of 20S proteasomes[15–17]. However, the biogenesis of 20S proteasomes remains largely elusive, especially in mammalian cells.

To identify proteins that interact with mammalian proteasomes, β1i subunits with a Flag tag were expressed in cells and anti-Flag immunoprecipitates were analysed by liquid chromatography coupled with tandem mass spectrometry[18]. We identified hUmp1 in addition to almost all of the subunits of 20S proteasomes and 19S regulatory complexes. We also identified two molecules with previously unknown relevance to proteasomes. One was Down syndrome critical region 2 (DSCR2), a small leucine-rich protein of 288 amino acids[19] that we have renamed PAC1. The other was a protein of 264 amino acids known as hepatocellular carcinoma associated gene 3 (HCCA3) (ref. 20), which we have renamed PAC2. Both PAC1 and PAC2 are ubiquitously expressed in mammals[19,20].

First, we confirmed that these molecules interact physically with proteasomes by transfecting Flag–PAC1 or Flag–PAC2 into HEK293T cells. The association increased on treatment of the cells with MG132, a proteasome inhibitor, in line with the increase in PAC1 and PAC2 expression (Supplementary Fig. 1a). Next, extracts of HeLa cells stably expressing Flag–PAC1 or Flag–PAC2 were fractionated by 8–32% glycerol gradient centrifugation. Both Flag–PAC1 and Flag–PAC2 were observed mainly in fractions containing sediments of precursor forms of proteasomes, as shown by the co-sedimentation of hUmp1, the unprocessed β1i (pro-β1i) subunit and α-subunits, and by the lack of chymotrypsin-like activity. Both Flag–PAC1 and Flag–PAC2 effectively co-precipitated with subunits from fraction 10 (Supplementary Fig. 1b, d). Moreover, even in fraction 16, which contained predominantly mature 20S proteasomes, they precipitated mainly with pro-β1i (Supplementary Fig. 1d), confirming that PAC1 and PAC2 associate specifically with precursor 20S proteasomes. Notably, the concentrations of precursor proteasomes were increased in both transfected cell lines (Supplementary Fig. 1c).

To examine the behaviour of endogenous PAC1 and PAC2 in detail, extracts from HEK293T cells were separated by lower density (4–24%) glycerol gradient centrifugation to resolve the precursor complexes. PAC1 and PAC2 were distributed mostly in the precursor fractions (Fig. 1a). Notably, the peaks of PAC1 and PAC2 were located in a fraction (fraction 12) lighter than that of the half-proteasomes (fraction 16), which contained hUmp1 and pro-β2. Moreover, the peaks of α5–α7 in precursor fractions were also located in fraction 12. Treatment with MG132 resulted in an accumulation of PAC1 and PAC2 in 20S proteasome fractions (Fig. 1a, right). The association of PAC1 and PAC2 with proteasomes was observed in fractions 12, 16 and 22 (Fig. 1b). When cells were treated with MG132, greater amounts of PAC1 and PAC2 were precipitated from fraction 22. Neither α4 nor α6 was associated with pro-β2 or hUmp1 in fraction 12. These results indicate that PAC1 and PAC2 form a complex with precursor 20S proteasomes before hUmp1 and the pro-β subunits are recruited, and suggest that PAC1 and PAC2 are chaperones for the maturation of 20S proteasomes and are released from or degraded by the newly assembled 20S proteasomes, analogous to the role of Ump1 in yeast[14].

To determine the composition of the peak of α-subunits that contained PAC1 and PAC2, fractions 12 and 16 were immunoprecipitated with antibodies against α6 and separated by two-dimensional polyacrylamide gel electrophoresis (2D-PAGE). Fraction 12 contained all seven α-subunits but no β-subunits, some of which were apparently detected in fraction 16 (Fig. 1c). Immunoblot analysis confirmed that all α-subunits except α1, which was difficult to distinguish by immunoblotting, were present in fraction 12 (Fig. 1d). The size of this complex (Fig. 1a), coupled with the absence of pro-β subunits or hUmp1 (Fig. 1a–c), means that it is

[1]Laboratory of Frontier Science, Core Technology and Research Center, Tokyo Metropolitan Institute of Medical Science, Bunkyo-ku, Tokyo 113-8613, Japan. [2]Institute of Molecular Biology and Physiology, University of Copenhagen, 13 Universitetsparken, DK 2100 Copenhagen, Denmark. [3]National Institute of Advanced Industrial Science and Technology, Biological Information Research Center, Kohtoh-ku, Tokyo 135-0064, Japan. [4]PRESTO, Japan Science and Technology Agency, Kawaguchi, Saitama 332-0012, Japan.

most probably a ring of all seven α-subunits, namely an α-ring. Immunoprecipitation in lower salt conditions showed that PAC1 and PAC2 are near-stoichiometric components of α-rings and that the association of PAC1 and PAC2 with α-subunits is salt labile (Fig. 1e, f). PAC1 was detected at a wide range of isoelectic point (pI) values, suggesting that it undergoes posttranslational modification (Fig. 1f). These results suggest that the PAC1–PAC2 complex and hUmp1 are distinct entities that work at different points in 20S proteasome assembly, and that PAC1 and PAC2 function as chaperone-like molecules at an earlier stage of 20S proteasome assembly relative to hUmp1.

Next, we characterized the interaction between PAC1 and PAC2. Coexpression of PAC1 and PAC2 in *Escherichia coli* and *in vitro* cotranscription–translation (IVTT) indicated that the two proteins bind directly (Supplementary Fig. 2a, b). Furthermore, PAC1 tagged with glutathione *S*-transferase (GST) pulled down PAC2 tagged with haemagglutinin A (HA) but not HA–PAC1, whereas GST–PAC2 pulled down HA–PAC1 but not HA–PAC2 *in vitro* (Supplementary Fig. 2b), indicating that PAC1 and PAC2 form hetero-oligomers but not homo-oligomers. No direct interaction between the PAC complex and hUmp1 was detected (Supplementary Fig. 2c). To determine the stoichiometry of the PAC complex, we coexpressed 3× Flag–PAC1 and 6× His–PAC2 in *E. coli* and purified the complex. PAC1 and PAC2 formed a complex at 1:1 stoichiometry with a relative molecular mass (M_r) corresponding to bovine serum albumin (67,000; Fig. 2a, b), indicating that the complex is a heterodimer.

To clarify further the nature of the PAC complex, we examined the half-lives of PAC1 and PAC2 by pulse-chase experiments. Both PAC1 and PAC2 turned over rapidly with similar half-lives of about 40 min (Fig. 2c). Treating the cells with MG132 markedly prolonged their half-lives, indicating that the PAC heterodimer is degraded by proteasomes. Because assembly of 20S proteasomes is complete within 1 h (ref. 21), the half-life of the PAC complex is consistent with the complex functioning as a chaperone for proteasome assembly and with its degradation on the completion of 20S proteasomes assembly.

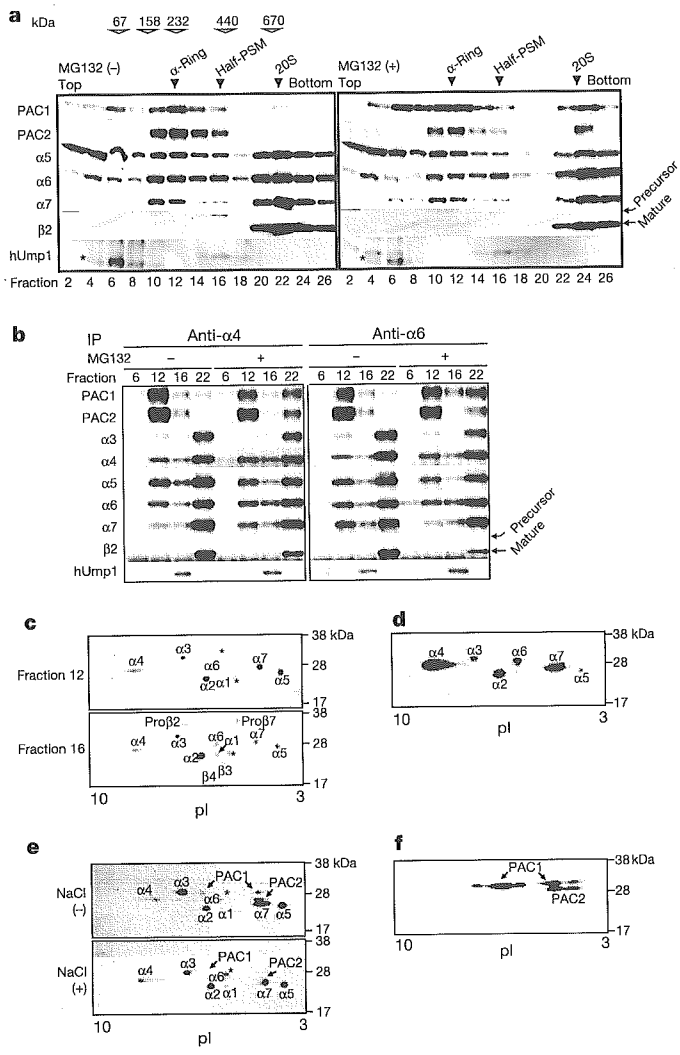

Figure 1 | PAC1 and PAC2 associate with precursor proteasomes. **a**, Glycerol gradient centrifugation (4–24%) of HEK293T cell extracts untreated or treated with MG132. Fractions were immunoblotted for the indicated proteins. Size markers and subcomplexes of proteasomes are indicated by open and filled arrowheads, respectively. Half-PSM indicates half-proteasomes. Asterisks indicate nonspecific bands. **b**, Fractions from **a** were immunoprecipitated with antibody against α4 or α6 and then subjected to immunoblotting. **c–f**, Fractions 12 (**c–f**) and 16 (**c**) from **a** were immunoprecipitated with beads conjugated to antibody against α6, washed with buffer A containing 150 mM (**c, d**), 0 mM or 50 mM (**e, f**) NaCl, eluted with glycine-HCl, and resolved by 2D-PAGE with silver (**c**) or Coomassie blue (**e**) staining. Asterisks denote unidentified spots. The top gel in **c** was immunoblotted with MCP231 and MCP34 antibodies against α-subunits and α4, respectively (**d**). The top gel in **e** was immunoblotted with antibodies against PAC1 and PAC2 (**f**). The non-uniformity of the spot intensity (**c, e**) may be due to a staining artefact because even in the half-proteasome fraction (fraction 16), which should contain all α-subunits in equal amounts, the spot intensities of α-subunits varied, resembling the pattern of fraction 12.

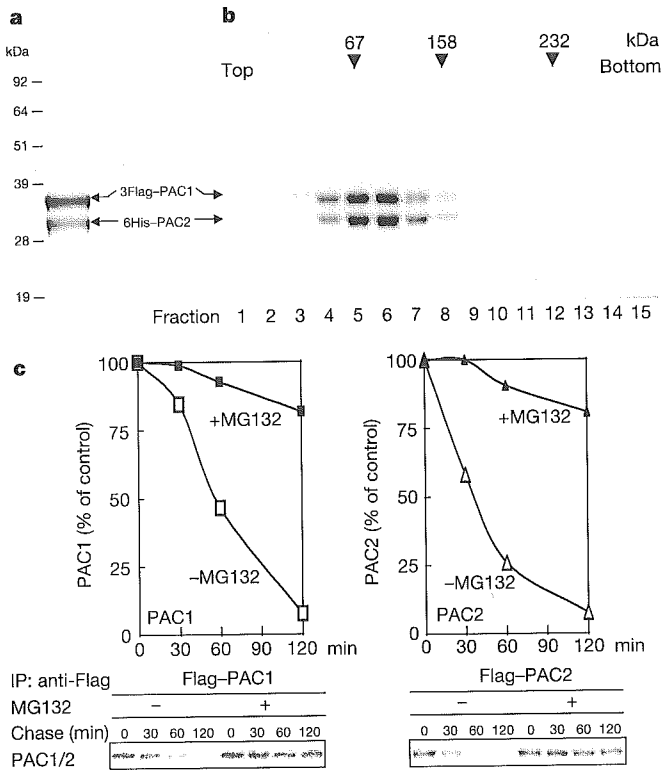

Figure 2 | The PAC1–PAC2 heterodimer is rapidly degraded by proteasomes. **a**, Coomassie blue staining of a copurified complex of 3× Flag–PAC1 and 6× His–PAC2 expressed in bacterial cells. **b**, The purified PAC complex in **a** was separated by 4–17% glycerol gradient centrifugation and subjected to SDS–PAGE with Coomassie staining. Arrowheads indicate size markers. **c**, Half-lives of PAC1 and PAC2. HeLa cells stably transfected with Flag–PAC1 or Flag–PAC2 were radiolabelled and chased in the presence or absence of MG132. Bottom panels show autoradiography; top panels show quantitative analysis of the bands.

To clarify the role of PAC1 and PAC2 in the assembly of the 20S proteasome *in vivo*, we used short interfering RNA (siRNA) to knock down the expression of PAC1 and PAC2. Knockdown of PAC1 resulted in loss of both PAC1 and PAC2 protein. Knockdown of PAC2 was also associated with a decrease in PAC1 protein (Fig. 3a), indicating that PAC1 and PAC2 are stable only when they form a heterodimer. Both PAC1- and PAC2-knockdown cells showed reduced proteolytic activity, as indicated by an assay of the antizyme-dependent degradation of ornithine decarboxylase (Supplementary Fig. 3a). Consequently, PAC-knockdown cells accumulated polyubiquitin-conjugated proteins, were sensitive to stress such as Cd^{2+}, and showed slow growth (Supplementary Fig. 3b–d).

We subjected the PAC-knockdown cells, as well as control and hUmp1-knockdown cells, to 4–24% glycerol gradient analysis. Notably, α-rings were hardly detected in either the PAC1- or the PAC2-knockdown cells (Fig. 3b). Instead, the α-subunits accumulated in fractions corresponding to half-proteasomes. This accumulation was not accompanied by an increase in pro-β2, pro-β5 or hUmp1, however, suggesting that the half-proteasomes were not normal. To confirm this notion, fraction 16 from the knockdown cells was immunoprecipitated with antibody against α6. Even though nearly equal amounts of α-subunits were loaded in the different samples, pro-β2, pro-β5 and hUmp1 were detected in much smaller amounts in PAC-knockdown cells (Fig. 3c), indicating that fraction 16 in PAC-knockdown cells contained mostly abnormally assembled α-subunits. This abnormal complex did not contain Rpt subunits, the components of 19S regulatory particles (Supplementary Fig. 3e, f), precluding the possibility that the mobility shift of α-subunits in PAC-knockdown cells was due to the premature association of α-subunits with Rpt subunits. On the basis of their sizes, these complexes are probably dimers of α-rings.

In hUmp1-knockdown cells, by contrast, we observed a marked reduction in 20S proteasomes but apparently normal α-rings and half-proteasomes, demonstrating the crucial role of hUmp1 in the dimerization of half-proteasomes. There was a strong increase in the free forms of some α-subunits in hUmp1-knockdown cells and a moderate increase in PAC-knockdown cells (Supplementary Fig. 3g). Assays of peptidase activities showed a significant reduction in activity of both the 20S and the 26S proteasome fractions in PAC-knockdown cells, although the effect of hUmp1 knockdown was more intense (Supplementary Fig. 3h). These data show definitively that the PAC complex has a pivotal role in the assembly of 20S proteasomes, specifically in keeping α-rings competent for the subsequent formation of half-proteasomes.

To elucidate the mechanism of PAC complex function, we tested the direct association of the complex with all of the subunits of 20S proteasomes. The PAC complex specifically interacted with α5 and α7, but not with other α-subunits or with any of the β-subunits *in vitro* (Supplementary Fig. 4a). Because Fig. 1a shows that the PAC1–PAC2 complex is found not only in α-ring fractions but also in lighter fractions, we considered whether it is involved in α-ring assembly. Immunoprecipitation with an antibody against Flag after the coexpression of all seven α-subunits, of which α5 was Flag-tagged, by IVTT showed that all α-subunits co-precipitated with Flag–α5 in larger amounts in the presence of the PAC complex than in its absence (Supplementary Fig. 4b). Immunoprecipitation with anti-Flag antibody after the coexpression of Flag–PAC1, PAC2 and α-subunits showed that PAC1 precipitated not only α5 and α7 but also all of the other α-subunits (Supplementary Fig. 4c), implying that it has a role in attracting α-subunits to each other.

We examined these interactions under more physiological conditions. Extracts of 293T cells that stably express Flag–PAC1 were separated by 4–24% glycerol gradient, and fractions corresponding to early α-subunit assembly intermediates and α-rings (fractions 8 and 12 in Fig. 1a, respectively) were immunoprecipitated with anti-Flag antibody and subjected to 2D-PAGE. PAC1 in fraction 12 co-precipitated all seven α-subunits, whereas PAC1 in fraction 8 co-precipitated several unidentified spots other than α-subunits, which made it difficult to identify α-subunits except for α5 and α7 by Coomassie staining (Fig. 4a, left). Immunoblot analysis showed that all α-subunits were present in the α-ring fraction, although α1 was difficult to distinguish (Fig. 4a, right), consistent with the findings in Fig. 1c. In contrast, PAC1 in fraction 8 co-precipitated a restricted set

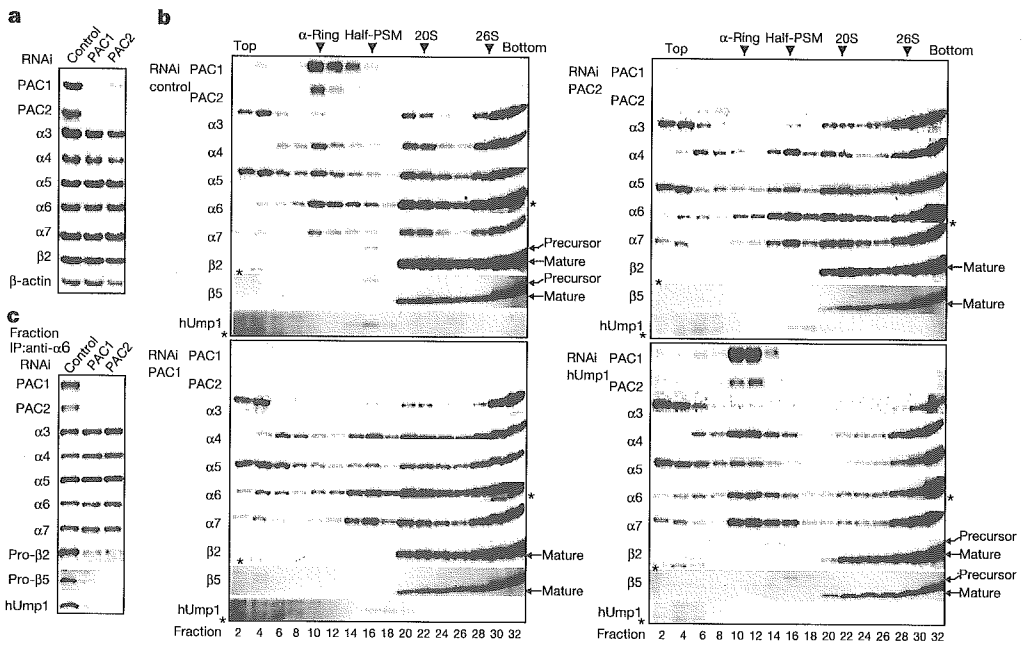

Figure 3 | siRNA-mediated knockdown of PAC1 and PAC2 impairs proteasome assembly. a–c, siRNA targeting PAC1 or PAC2, or control siRNA, was transfected into HEK293T cells. Knockdown of hUmp1 was also analysed in **b**. Whole-cell extracts (**a**), fractions separated by 4–24% glycerol gradient centrifugation (**b**), and immunoprecipitates obtained from fraction 16 in **b** with antibodies against α6 (**c**) were immunoblotted for the indicated proteins. Asterisks indicate nonspecific bands.

of α-subunits in which α3 and α4 were hardly detected. These results indicate that there is a hierarchy among α-subunits in their incorporation into α-rings, and that the PAC complex associates with the α-subunits before α-rings are complete, and functions as a scaffold for α-ring assembly.

Finally, we tested whether the complex of α-subunits in fraction 12 is a unique species. The affinity-purified complex from fraction 12 was subjected to native-PAGE. We found that the complex had a unique electrophoretic mobility (Fig. 4b). Moreover, the complex was eluted with a single sharp peak by anion-exchange chromatography (Fig. 4c). Thus, this complex is a unique species biochemically and is a genuine α-ring rather than a group of heterogeneous and incomplete α-ring precursors.

Our present work provides a model in which the chaperone complex PAC1–PAC2 mediates the formation of α-rings, keeps the rings competent for half-proteasome formation, and is required for proper proteasome maturation and cellular integrity (Fig. 4d). (See Supplementary Discussion for a more detailed description.)

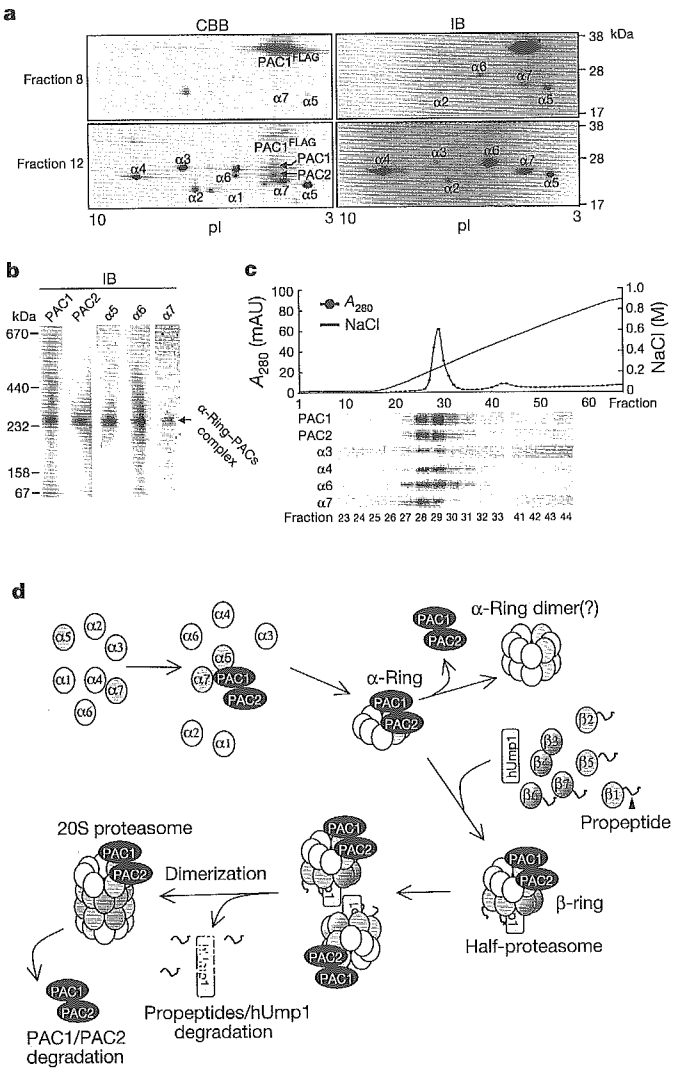

Figure 4 | PAC1–PAC2 provides a scaffold for α-ring formation. **a**, Extracts of HEK293T cells transfected with Flag–PAC1 were fractionated as in Fig. 1a. The Flag–PAC1 complexes from fractions 8 and 12 were purified with M2 agarose, resolved by 2D-PAGE and detected by Coomassie blue staining (left) or immunoblotting as in Fig. 1d (right). Asterisks denote unidentified spots. **b**, **c**, Purified Flag–PAC1 complex from fraction 12 was subjected to native-PAGE (**b**) or anion-exchange chromatography (**c**), followed by immunoblotting. **d**, Multistep model of the ordered assembly of mammalian 20S proteasomes. Some of the newly synthesized free α-subunits bind to the PAC1–PAC2 heterodimer, which provides a scaffold for α-ring formation, thereby suppressing the off-pathway aggregation of α-subunits and keeping α-rings competent for half-proteasome formation. Two half-proteasomes then dimerize, the β-subunits are processed and hUmp1 is degraded. The PAC1–PAC2 complex is subsequently degraded by the newly formed active 20S proteasomes.

METHODS

See Supplementary Methods for procedures used in the experiments in Supplementary Figs 1–4.

DNA constructs and cell culture. We synthesized cDNAs encoding PAC1, PAC2, hUmp1 and proteasome α- and β-subunits from total RNA isolated from HeLa cells using Superscript II (Invitrogen). PCR was carried out on the cDNA with Pyrobest DNA polymerase (Takara). All of the amplified fragments were cloned into pcDNA3.1 (Invitrogen) and sequenced for confirmation. For expression of GST fusion proteins, the cDNAs were subcloned into pGEX6P-1 (Amersham). Transfections of 293T cells were done with Fugene 6 (Roche). Stable transfections of HeLa cells or 293T cells were done with Lipofectamine 2000 (Invitrogen), and the cells were selected with 1 mg ml^{-1} of G418 or 5 μg ml^{-1} of puromycin, respectively. We used 20 μM MG132 (Peptide Institute) to inhibit proteasome activities 2 h before the cells were collected.

Protein extracts, immunological analysis and antibodies. Cells were lysed in ice-cold buffer A containing 50 mM Tris-HCl (pH 7.5), 0.5% (v/v) Nonidet P40, 1 mM dithiothreitol (DTT) and 2 mM ATP, and the extracts were clarified by centrifugation at 20,000*g* for 10 min at 4 °C. SDS–PAGE (12% gel or 4–12% gradient Bis-Tris gel; Invitrogen) and native-PAGE (3–8% gradient Tris-acetate gel; Invitrogen) were done in accordance with the manufacturer's instructions. The separated proteins were transferred onto polyvinylidene difluoride membrane and reacted with the indicated antibody. Development was done with Western Lighting reagent (Perkin Elmer). Polyclonal antibodies against hUmp1, PAC1 and PAC2 were raised in rabbits using a synthetic peptide (E_{115}DILNDPSQSE_{125}), and recombinant PAC1 and PAC2 protein, respectively. PAC1 and PAC2 were produced and purified as GST fusion proteins, and GST was removed by PreScission protease (Amersham).

Antibodies against proteasome α3 subunit (MCP257), α4 (MCP34), α5 (MCP196), α6 (MCP20), α7 (MCP72), β2 (MCP168) and α-subunits (MCP231, which reacts with all α-subunits except α4) were purchased from BioMol. Antibodies against β5 (P93250), β6 (P93199) and β1i were prepared as described[22]. We used antibodies against the Flag tag (Sigma) and β-actin (Chemicon), and horseradish peroxidase (HRP)-conjugated rabbit anti-mouse and goat anti-rabbit IgG (Jackson ImmunoResearch) for immunodetection. For immunoprecipitation of the Flag epitope, we used M2 agarose (Sigma). For immunoprecipitation of proteasomes, we used antibody MCP34 or MCP20 bound to protein G Sepharose (Amersham). In the experiments in Fig. 1c–f, we used MCP20 crosslinked to NHS-activated Sepharose (Amersham). These beads were added to the extracts, mixed under constant rotation for 2 h at 4 °C, washed four times with buffer A (except in the experiments in Fig. 1c–f), and boiled in SDS sample buffer, or eluted with 100 μg ml^{-1} of Flag peptides (Sigma) or with 0.2 M glycine-HCl (pH 2.8). Densitometric analysis was done with Image Gauge software (Fujifilm). 2D-PAGE was done as described[23].

Glycerol gradient analysis. Samples and molecular weight markers (Amersham) were fractionated by 4–17% (v/v), 4–24% (v/v) or 8–32% (v/v) linear glycerol density gradient centrifugation (22 h, 100,000*g*) as described[22].

Purification of PAC1–PAC2 complex. We coexpressed 3× FLAG–PAC1 and 6× His–PAC2 in *E. coli* using a pRSFDuet-1 vector (Novagen). The cell pellets were lysed in buffer B containing 20 mM sodium phosphate (pH 7.8), 500 mM NaCl and 1.0% Triton X-100, and sonicated. Ni-NTA Sepharose (Qiagen) was added to the extracts, which were then washed with buffer C containing 20 mM sodium phosphate (pH 6.0) and 500 mM NaCl, and eluted with buffer C plus 100 mM imidazole. The eluted products were further purified with M2 agarose and eluted with 100 μg ml^{-1} of Flag peptide (Sigma).

Pulse-chase experiments. Cells were incubated with methionine-free medium for 1 h, metabolically labelled with ^{35}S-methionine for 1 h, and then washed and chased for the indicated time. The cell lysates were immunoprecipitated with M2 agarose, fractionated by SDS–PAGE and visualized by autoradiography.

RNAi experiments. siRNAs targeting human PAC1, PAC2 and hUmp1 with the following 19-nucleotide sequences were designed by B-Bridge and synthesized by Dharmacon: PAC1, 5′-CCAGAAGCUUGAAGGGUUU-3′; PAC2, 5′-GCAUAAAUGCUGAAGUGUA-3′; hUmp1, a mixture of 5′-GCAAGUGG ACCUUUUGAAA-3′ and 5′-CCUGAGAAUUUCUGCUCAA-3′. Control siRNA (Non-specific Control Duplex VIII) was purchased from B-Bridge. Transfections of siRNAs into HEK293T cells were done with Lipofectamine

2000 at a final concentration of 50 nM in six-well dishes. The cells were analysed 72 h after transfection.

Assay of proteasome activity. Peptidase activity was measured by using a fluorescent peptide substrate, succinyl-Leu-Leu-Val-Tyr-7-amido-4-methyl-coumarin (Suc-LLVY-MCA), as described[23].

Chromatography. Anion-exchange chromatography was done with a Resource Q column (Amersham). Bound proteins were eluted with a salt gradient of 0–1 M NaCl in a buffer containing 50 mM Tris-HCl (pH 8.0), 1 mM DTT and 5% glycerol.

Received 27 June; accepted 2 August 2005.

1. Pickart, C. M. Mechanisms underlying ubiquitination. *Annu. Rev. Biochem.* **70**, 503–533 (2001).
2. Glickman, M. H. & Ciechanover, A. The ubiquitin–proteasome proteolytic pathway: destruction for the sake of construction. *Physiol. Rev.* **82**, 373–428 (2002).
3. Baumeister, W., Walz, J., Zuhl, F. & Seemuller, E. The proteasome: paradigm of a self-compartmentalizing protease. *Cell* **92**, 367–380 (1998).
4. Groll, M. *et al.* Structure of 20S proteasome from yeast at 2.4 Å resolution. *Nature* **386**, 463–471 (1997).
5. Unno, M. *et al.* The structure of the mammalian 20S proteasome at 2.75 Å resolution. *Structure (Camb.)* **10**, 609–618 (2002).
6. Zwickl, P., Kleinz, J. & Baumeister, W. Critical elements in proteasome assembly. *Nat. Struct. Biol.* **1**, 765–770 (1994).
7. Gerards, W. L. *et al.* The human α-type proteasomal subunit HsC8 forms a double ringlike structure, but does not assemble into proteasome-like particles with the β-type subunits HsDelta or HsBPROS26. *J. Biol. Chem.* **272**, 10080–10086 (1997).
8. Yao, Y. *et al.* α5 subunit in *Trypanosoma brucei* proteasome can self-assemble to form a cylinder of four stacked heptamer rings. *Biochem. J.* **344**, 349–358 (1999).
9. Yang, Y., Fruh, K., Ahn, K. & Peterson, P. A. *In vivo* assembly of the proteasomal complexes, implications for antigen processing. *J. Biol. Chem.* **270**, 27687–27694 (1995).
10. Chen, P. & Hochstrasser, M. Autocatalytic subunit processing couples active site formation in the 20S proteasome to completion of assembly. *Cell* **86**, 961–972 (1996).
11. Schmidtke, G. *et al.* Analysis of mammalian 20S proteasome biogenesis: the maturation of β-subunits is an ordered two-step mechanism involving autocatalysis. *EMBO J.* **15**, 6887–6898 (1996).
12. Nandi, D., Woodward, E., Ginsburg, D. B. & Monaco, J. J. Intermediates in the formation of mouse 20S proteasomes: implications for the assembly of precursor β subunits. *EMBO J.* **16**, 5363–5375 (1997).
13. Schmidtke, G., Schmidt, M. & Kloetzel, P. M. Maturation of mammalian 20 S proteasome: purification and characterization of 13 S and 16 S proteasome precursor complexes. *J. Mol. Biol.* **268**, 95–106 (1997).
14. Ramos, P. C., Hockendorff, J., Johnson, E. S., Varshavsky, A. & Dohmen, R. J. Ump1p is required for proper maturation of the 20S proteasome and becomes its substrate upon completion of the assembly. *Cell* **92**, 489–499 (1998).
15. Griffin, T. A., Slack, J. P., McCluskey, T. S., Monaco, J. J. & Colbert, R. A. Identification of proteassemblin, a mammalian homologue of the yeast protein, Ump1p, that is required for normal proteasome assembly. *Mol. Cell. Biol. Res. Commun.* **3**, 212–217 (2000).
16. Witt, E. *et al.* Characterisation of the newly identified human Ump1 homologue POMP and analysis of LMP7(β5i) incorporation into 20 S proteasomes. *J. Mol. Biol.* **301**, 1–9 (2000).
17. Burri, L. *et al.* Identification and characterization of a mammalian protein interacting with 20S proteasome precursors. *Proc. Natl Acad. Sci. USA* **97**, 10348–10353 (2000).
18. Natsume, T. *et al.* A direct nanoflow liquid chromatography-tandem mass spectrometry system for interaction proteomics. *Anal. Chem.* **74**, 4725–4733 (2002).
19. Vidal-Taboada, J. M. *et al.* Down syndrome critical region gene 2: expression during mouse development and in human cell lines indicates a function related to cell proliferation. *Biochem. Biophys. Res. Commun.* **272**, 156–163 (2000).
20. Bahar, R. *et al.* Growth retardation, polyploidy, and multinucleation induced by Clast3, a novel cell cycle-regulated protein. *J. Biol. Chem.* **277**, 40012–40019 (2002).
21. Ahn, K. *et al. In vivo* characterization of the proteasome regulator PA28. *J. Biol. Chem.* **271**, 18237–18242 (1996).
22. Tanahashi, N. *et al.* Hybrid proteasomes. Induction by interferon-γ and contribution to ATP-dependent proteolysis. *J. Biol. Chem.* **275**, 14336–14445 (2000).
23. Murata, S. *et al.* Immunoproteasome assembly and antigen presentation in mice lacking both PA28α and PA28β. *EMBO J.* **20**, 5898–5907 (2001).

Supplementary Information is linked to the online version of the paper at www.nature.com/nature.

Acknowledgements We thank Y. Murakami for the ornithine decarboxylase degradation assay system, K. Furuyama for technical support, and D. Finley for comments on the manuscript. This work was supported by grants from the Japanese Science and Technology Agency (to S.M.), the Ministry of Education, Science and Culture of Japan (to S.M. and K.T.) and the New Energy and Industrial Technology Development Organization (to T.N.). Y.H. was supported by the Japanese Society for the Promotion of Science.

Author Information The sequences for human PAC1 and PAC2 have been deposited in GenBank under accession numbers BR000236 and BR000237, respectively. Reprints and permissions information is available at npg.nature.com/reprintsandpermissions. The authors declare no competing financial interests. Correspondence and requests for materials should be addressed to S.M. (smurata@rinshoken.or.jp) or K.T. (tanakak@rinshoken.or.jp).

The EMBO Journal (2006) 25, 211–221 | © 2006 European Molecular Biology Organization | All Rights Reserved 0261-4189/06
www.embojournal.org

THE EMBO JOURNAL

14-3-3η is a novel regulator of parkin ubiquitin ligase

Shigeto Sato[1,2], Tomoki Chiba[2], Eri Sakata[3], Koichi Kato[3], Yoshikuni Mizuno[1], Nobutaka Hattori[1] and Keiji Tanaka[2,*]

[1]Department of Neurology, Juntendo University School of Medicine, Bunkyo, Tokyo, Japan, [2]Tokyo Metropolitan Institute of Medical Science, Bunkyo-ku, Tokyo, Japan and [3]Department of Structural Biology and Biomolecular Engineering, Graduate School of Pharmaceutical Sciences, Nagoya City University, Mizuho-ku, Nagoya, Japan

Mutation of the *parkin* gene, which encodes an E3 ubiquitin-protein ligase, is the major cause of autosomal recessive juvenile parkinsonism (ARJP). Although various substrates for parkin have been identified, the mechanisms that regulate the ubiquitin ligase activity of parkin are poorly understood. Here we report that 14-3-3η, a chaperone-like protein present abundantly in neurons, could bind to parkin and negatively regulate its ubiquitin ligase activity. Furthermore, 14-3-3η could bind to the linker region of parkin but not parkin with ARJP-causing R42P, K161N, and T240R mutations. Intriguingly, α-synuclein (α-SN), another familial Parkinson's disease (PD) gene product, abrogated the 14-3-3η-induced suppression of parkin activity. α-SN could bind tightly to 14-3-3η and consequently sequester it from the parkin–14-3-3η complex. PD-causing A30P and A53T mutants of α-SN could not bind 14-3-3η, and failed to activate parkin. Our findings indicate that 14-3-3η is a regulator that functionally links parkin and α-SN. The α-SN-positive and 14-3-3η-negative control of parkin activity sheds new light on the pathophysiological roles of parkin.

The EMBO Journal (2006) **25**, 211–221. doi:10.1038/sj.emboj.7600774; Published online 11 August 2005
Subject Categories: proteins; molecular biology of disease
Keywords: α-synuclein; 14-3-3η; parkin; Parkinson's disease; ubiquitin ligase

Introduction

In the last decade, people working in the field of Parkinson's disease (PD) witnessed a tremendous progress in uncovering the mechanisms of PD, and several familial PD genes were discovered in succession (Vila and Przedborski, 2004). Of these hereditary PD genes, *parkin* (*PARK2*), the causative gene of autosomal recessive juvenile parkinsonism (ARJP), is of a special interest because it encodes a ubiquitin ligase, a critical component of the pathway that covalently attaches ubiquitin to specific proteins with a polymerization step to form a degradation signal (Shimura *et al*, 2000). Indeed, parkin catalyzes the addition of ubiquitin to target proteins prior to their destruction via the proteasome, suggesting that the misregulation of proteasomal degradation of parkin substrate(s) is deleterious to dopaminergic neurons (Dawson and Dawson, 2003; Bossy-Wetzel *et al*, 2004; Kahle and Haass, 2004). Consequently, impaired protein clearance can induce dopaminergic cell death, supporting the concept that defects in the ubiquitin–proteasome system may underlie nigral degeneration in ARJP and perhaps sporadic forms of PD (McNaught and Olanow, 2003). On the other hand, it was recently reported that parkin also catalyzes the formation of the K63-linked polyubiquitylation chain, independent of proteasomal destruction, in which the K48-linked polyubiquitylation chain is necessary (Doss-Pepe *et al*, 2005; Lim *et al*, 2005). Thus, it is plausible that parkin shares two roles as an E3 ligase; that is, one linking to and the other independent of the proteasome.

Among the products of major familial PD genes (Vila and Przedborski, 2004), α-synuclein (α-SN) is a product of familial PD gene (*PARK1*) identified as a presynaptic protein of unknown function. α-SN is considered in the molecular mechanisms of PD mainly because it is one of the major components of the cytoplasmic Lewy body (LB) inclusion present in the remaining nigral dopaminergic neurons of PD patients, which is the pathological hallmark of sporadic and some familial PDs (Forno, 1996). Although various studies have been conducted on α-SN (Dawson and Dawson, 2003; Bossy-Wetzel *et al*, 2004; Kahle and Haass, 2004), its pathophysiological role(s) and the interplay between α-SN and parkin are largely unknown.

To date, little is known about the role of parkin as a ubiquitin E3 ligase with respect to the underlying molecular mechanism(s) of ARJP or PD. Here we report for the first time that 14-3-3η, a member of the 14-3-3 family (β/α, γ, ε, η, ζ/δ, σ, and τ/θ) (Berg *et al*, 2003; Bridges and Moorhead, 2004; Mackintosh, 2004) identified in LB (Kawamoto *et al*, 2002; Ubl *et al*, 2002), binds primarily to the linker region of parkin and functions as a novel negative regulator of parkin. We also show that α-SN relieves parkin activity suppressed by 14-3-3η, indicating that 14-3-3η is a novel molecule handling both parkin and α-SN, and that functionally links the two familial PD gene products.

Results

Parkin specifically interacts with 14-3-3η but not with other 14-3-3 isoforms

We first examined the physical association of parkin with 14-3-3 isoforms, which are abundantly expressed in the brain (Martin *et al*, 1994; Baxter *et al*, 2002). Parkin was immunoprecipitated from mouse brain extracts, and the presence of 14-3-3 was analyzed by Western blotting (Figure 1A). 14-3-3 was clearly detected in the parkin immunoprecipitant, but not in those of control IgG or parkin antibody preabsorbed

*Corresponding author. Department of Molecular Oncology, The Tokyo Metropolitan Institute of Medical Science, 3-18-22 Honkomagome, Bunkyo-ku, Tokyo 113-8613, Japan. Tel./Fax: +81 3 3823 2237; E-mail: tanakak@rinshoken.or.jp

Received: 24 January 2005; accepted: 15 July 2005; published online: 11 August 2005

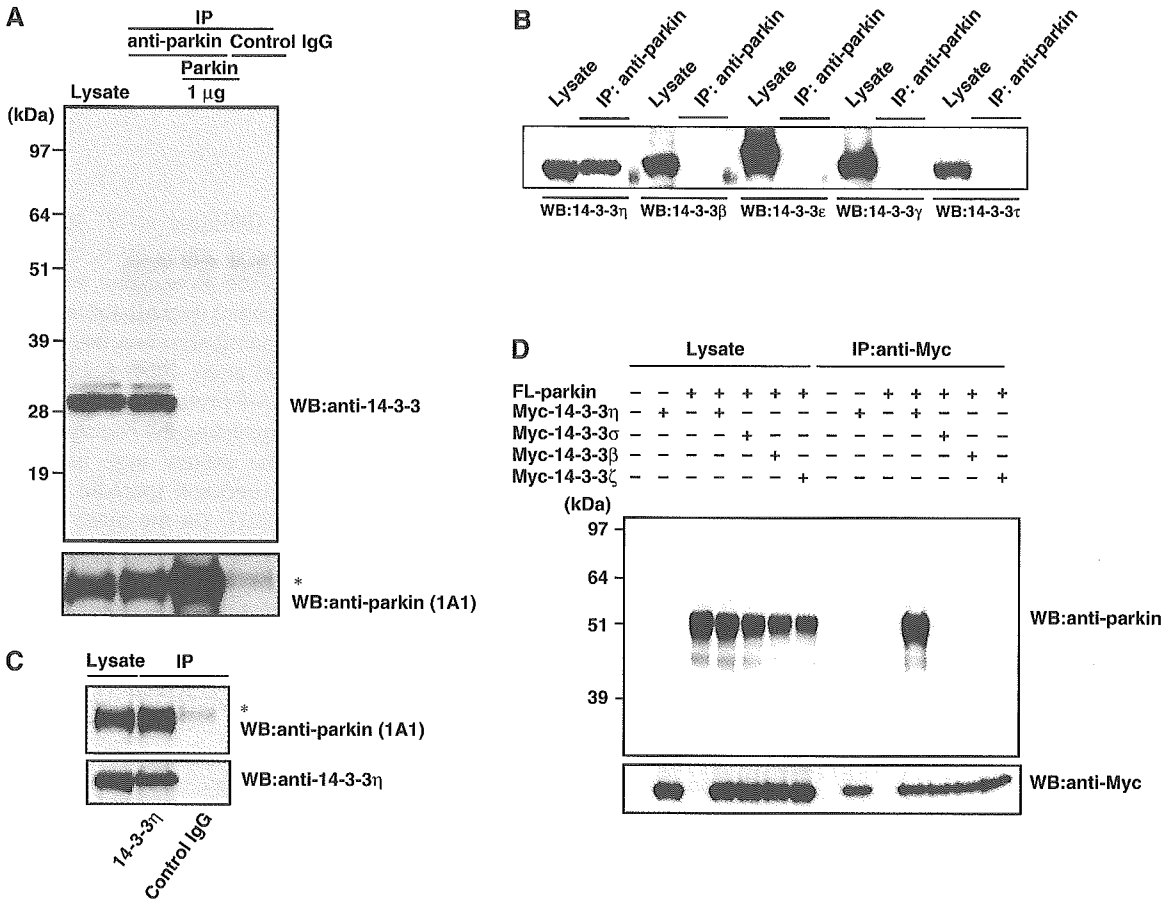

Figure 1 Physical interaction between parkin and 14-3-3η. (**A**) Immunoprecipitation by anti-parkin antibody in the mouse brain. Mouse brain lysates were prepared and treated with anti-parkin or control IgG as described in Materials and methods. The resulting immunoprecipitates were subjected to SDS–PAGE, followed by Western blotting with anti-14-3-3 and parkin (1A1) antibodies. In all, 1 μg of recombinant parkin was pretreated with anti-parkin prior to immunoprecipitation. Left lane: the brain lysate (1.5% input). Asterisk denotes an IgG heavy chain. (**B**) Specificity analysis of 14-3-3 species. The immunoprecipitation with anti-parkin and subsequent SDS–PAGE were carried out as in (A). Western blotting was conducted with antibodies against various 14-3-3 isoforms as indicated for lysates and anti-parkin immunoprecipitates. (**C**) Immunoprecipitation by anti-14-3-3η antibody. After immunoprecipitation with anti-14-3-3η or control IgG of the brain lysate, the immunoprecipitates were analyzed by Western blotting with anti-parkin (1A1) and 14-3-3η antibodies, similar to (A). Left lane: the brain lysate (1.5% input). Asterisk denotes an IgG heavy chain. (**D**) Interaction between parkin and 14-3-3η in HEK293 cells. FL-parkin (5 μg), Myc-14-3-3η, σ, β, or ζ (2 μg) plasmids were transfected as indicated into HEK293 cells. After 48 h, the cell lysate was prepared and used for immunoprecipitation with anti-Myc antibody. The immunoprecipitates and the lysate (7.5% input) were analyzed by Western blotting with anti-parkin and Myc antibodies, as in (A).

with recombinant parkin protein (1 μg). Intriguingly, two 14-3-3 signals were evident: a faint band and a strongly stained band, indicating that the 14-3-3 may form homo- and/or hetero-dimers. Subsequently, we determined the type(s) of 14-3-3 species that interacts with parkin in the mouse brain in more detail. In the parkin immunoprecipitant, 14-3-3η, but not other 14-3-3 isoforms examined, that is, β, γ, ε, and τ, was detected (Figure 1B). In the next step, we examined whether parkin is coimmunoprecipitated with anti-14-3-3η antibody and found parkin in the 14-3-3η immunoprecipitant (Figure 1C). These reciprocal immunoprecipitation experiments revealed that parkin is associated with 14-3-3η in the mouse brain.

To confirm the specific interaction of parkin with 14-3-3η, Myc-tagged 14-3-3η, σ, β, or ζ was cotransfected with FLAG (FL)-parkin into HEK293 cells, and their interactions were tested. FL-parkin was detected in the immunoprecipitant of Myc-14-3-3η, but not those of Myc-14-3-3σ, β, and ζ (Figure 1D). Taken together with the results of Figure 1B, our data indicate that parkin mainly interacts with 14-3-3η.

Parkin domain interacts with 14-3-3η

We next investigated the region of parkin necessary for interaction with 14-3-3η. Structurally, parkin is characterized by the presence of the N-terminal ubiquitin-like domain (UBL) (which is highly homologous to ubiquitin), the C-terminal RING box, consisting of two RING finger motifs, RING1 and RING2, flanked by one IBR (in between RING finger) motif, and a linker region, which connects these N- and C-terminal regions (Shimura *et al*, 2000). In these experiments, various deletion mutants of FL-tagged parkin were expressed in HEK293 cells and immunoprecipitated by FL-antibody beads (Figure 2A). FL-parkin or its derivatives on the beads were further incubated with cell lysates that expressed Myc-14-3-3η, and then the amounts of Myc-14-3-3η bound to the beads were determined (Figure 2B).

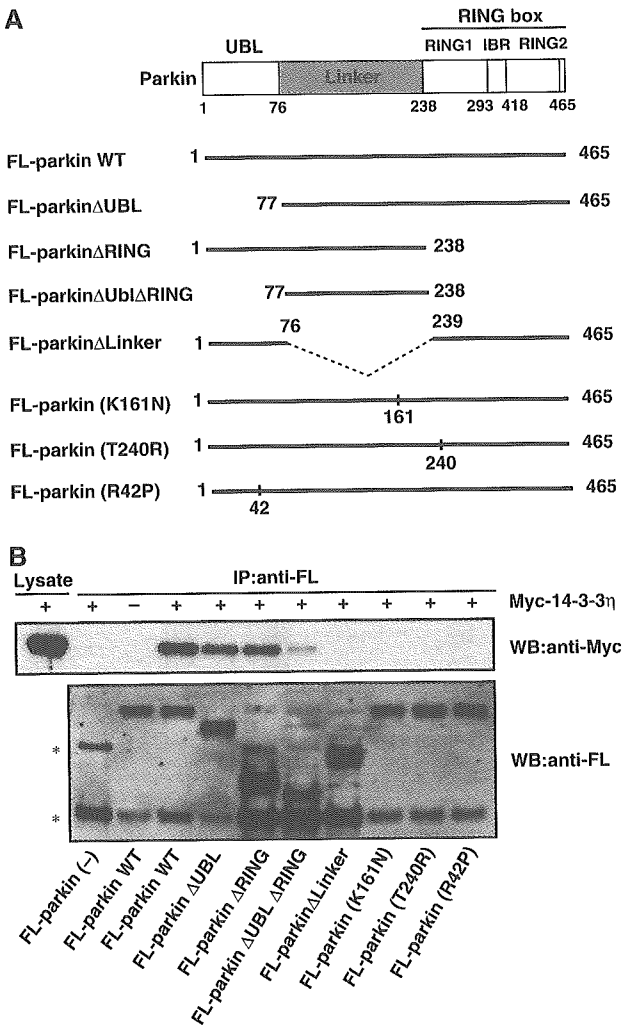

Figure 2 Domain analysis of the parkin region that interacts with 14-3-3η. (**A**) Schematic representation of WT parkin and its deletion- and disease-related missense mutants. See text for the domain structures of parkin and mutants. The dotted line denotes the deleted region. (**B**) Interaction between 14-3-3η and parkin mutants. FL-parkin (2 μg) or its mutant (10 μg) plasmids were transfected into HEK293 cells, as described in Figure 1D. The cell lysates (200–600 μl) were immunoprecipitated with anti-FL-antibody beads. Note that various amounts of the lysates were used to adjust roughly the levels of expressed parkin mutants. The resulting immunoprecipitates were mixed with other cell lysates (200 μl) prepared from cells that had been transfected with Myc-14-3-3η plasmid (2 μg) and incubated for 6 h at 4°C. Then, the extensively washed immunoprecipitates and cell lysate (7.5% input) were analyzed by Western blotting with anti-Myc and FL antibodies. Asterisks denote nonspecific bands.

The full-length parkin could bind 14-3-3η. Deletion of either UBL or RING-box domain reduced the binding compared to the full-length parkin, although these deletion mutants retained the ability to bind to 14-3-3η. Furthermore, mutants with combined deletions of the UBL and RING-box domains, that is, the linker region, could also bind 14-3-3η to a lesser extent. Conversely, deletion of the linker region resulted in the loss of ability to bind 14-3-3η. Taken together, it is concluded that the linker region is necessary for the interaction between parkin and 14-3-3η, although the UBL and RING-box domains may enhance the binding affinity.

Interestingly, the ARJP disease-causing missense mutation within the linker region, that is, parkin(K161N), in which the Lys residue at position 161 was replaced by Asn residue, showed complete loss of binding to 14-3-3η, confirming the importance of the linker region in the interaction between 14-3-3η and parkin. Unexpectedly, other disease-causing missense mutations of the UBL region, parkin(R42P), and the RING1 region, parkin(T240R), also showed complete loss of interaction with 14-3-3η (Figure 2). Thus, although the UBL and RING-box domains are not primarily required for the binding, both R42P and T240R mutations in the UBL and RING-box domains, respectively, deleteriously affect the neighboring linker domain. Alternatively, since 14-3-3 is known to form a homo- or hetero-dimer, and thus has two binding sites (Aitken *et al*, 2002), it is plausible that 14-3-3η interacts with two distinct regions of parkin, one major site of which is the linker region.

Effect of suppression of 14-3-3η on parkin E3 activity

We next investigated the role of parkin–14-3-3η binding on parkin activity. At first, we tested its effect on the ubiquitin ligase activity of parkin. We incubated recombinant His-parkin with ubiquitin, E1, and E2 (UbcH7) *in vitro*. Under this condition, His-parkin appeared as a smear band, which likely reflects self-ubiquitylation (Figure 3A). Addition of recombinant GST-14-3-3η (Figure 3A, left panel) or untagged 14-3-3η (Figure 3A, right panel) to the reaction reduced the smear of His-parkin, and such reduction was proportionate to the added amount of GST-14-3-3η or 14-3-3η and resulted in the recovery of His-parkin of intact size. In addition, we found that 14-3-3η had no effect on the ubiquitylating activity of phosphorylated IκBα by a fully *in vitro* reconstituted system, containing E1, E2 (Ubc4), and E3 (the $SCF^{\beta TrCP}$ complex; Kawakami *et al*, 2001), indicating that 14-3-3η does not interfere with ubiquitylating reactions in general (data not shown). These results strongly suggest that 14-3-3η suppresses the intrinsic self-ubiquitylation activity of parkin.

We next tested whether 14-3-3η also affects the ubiquitylation activity of parkin in HEK293 cells. First, we examined the self-ubiquitylation of parkin, whose activity was observed by cotransfections of HA-ubiquitin and FL-parkin. Myc-14-3-3η almost completely suppressed the self-ubiquitylation activity of parkin, while Myc-14-3-3σ, β, and ζ had no inhibitory effect (Figure 3B), indicating the specific role of 14-3-3η for parkin. Second, we examined the effect of 14-3-3η on the ubiquitylation of a model substrate for parkin. When V5-tagged synphilin-1, a known parkin substrate (Chung *et al*, 2001), was transfected with FL-parkin and HA-ubiquitin in the cells, V5-synphilin-1 was found in ubiquitylated form, as demonstrated by the poly-ubiquitin chain formation (detected by anti-HA antibody) in anti-V5 immunoprecipitant (Figure 3C, top panel). V5-synphilin-1 was not ubiquitylated when FL-parkin was not cotransfected, suggesting that this ubiquitylation is mediated by coexpressed FL-parkin. Indeed, FL-parkin was found to be associated with V5-synphilin-1, further supporting the above notion (Figure 3C, second panel from the top). Note that the polyubiquitylated bands observed as the smear profile were considered to include not only major synphilin-1 bands over 90-kDa size but also self-ubiquitylated bands of parkin over 52-kDa size.

In the next step, we tested the effects of 14-3-3η on the ubiquitylation and binding activities of parkin to

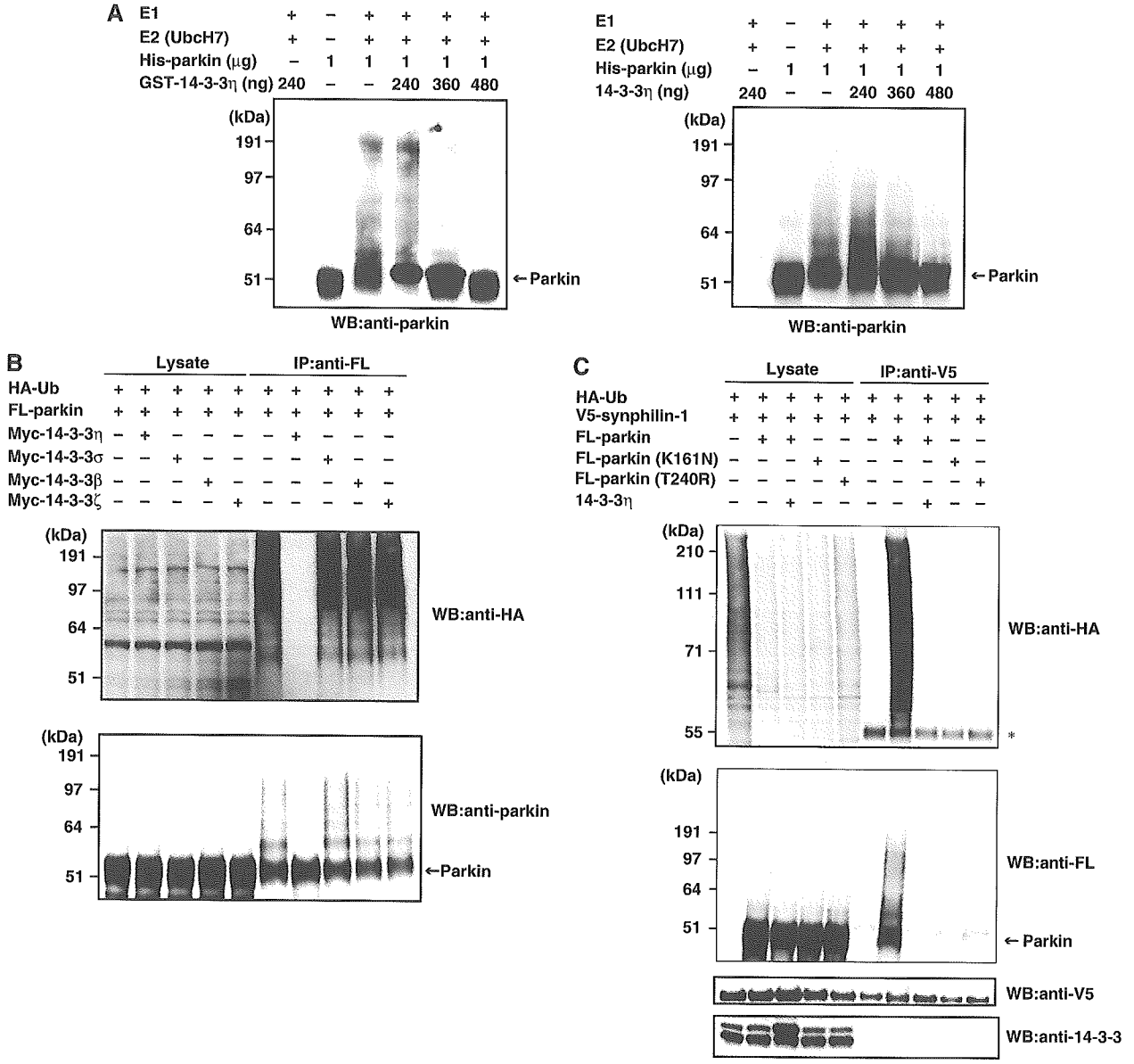

Figure 3 Effects of 14-3-3η on the E3 activity of parkin. (**A**) *In vitro* autoubiquitylation. The ubiquitylating assay was conducted as described in Materials and methods with or without various amounts of GST-14-3-3η (left panel) or 14-3-3η (right panel). After incubation, the reaction mixtures were subjected to SDS–PAGE, followed by Western blotting with anti-parkin. Arrow on the right indicates the position of His-parkin. (**B**) *In vivo* autoubiquitylation. HA-Ub (3 μg), FL-parkin (3 μg), and Myc-14-3-3η, σ, β, or ζ (6 μg) plasmids were transfected for 48 h into HEK293 cells as indicated. After immunoprecipitation with anti-FL, Western blotting was performed using antibodies against HA and parkin. Western blotting of all lysates was performed to test the expression levels (Lysate). (**C**) Ubiquitylation of synphilin-1 in HEK293 cells. HA-Ub (2 μg), FL-parkin (3 μg), FL-parkin(K161N) (3 μg), FL-parkin(T240R) (3 μg), Myc-14-3-3η (6 μg), and V5-synphilin-1 (4 μg) plasmids were transfected into HEK293 cells as in (B) at the indicated combinations. After immunoprecipitation with anti-V5 antibody, Western blotting was performed using antibodies against HA, FL, V5, and 14-3-3. Asterisk denotes an IgG heavy chain.

V5-synphilin-1. Cotransfection of 14-3-3η resulted in almost complete inhibition of the ubiquitylation of synphilin-1 by parkin and/or self-ubiquitylation of parkin (Figure 3C, top and second panels), as well as inhibition of the interaction between synphilin-1 and parkin (Figure 3C, second panel). 14-3-3η did not interact with synphilin-1 (Figure 3C, bottom panel). Taken together, these results suggest that 14-3-3η does not only inhibit the intrinsic ubiquitylation activity of parkin, but also its binding activity to the substrate and its ubiquitylation.

The ARJP disease-related parkin(K161N) and parkin(T240R) mutants, which cannot bind with 14-3-3η, could not bind and ubiquitylate synphilin-1 and/or self-ubiquitylation of parkin even in the absence of 14-3-3η (Figure 3C, top panel). Hence, the linker and RING-box domains of parkin are essential not only for the negative regulation by 14-3-3η, but also for the substrate recognition and ubiquitin-ligase activity. These results illustrate the importance of these regions of parkin on its positive and negative regulation.

Since parkin is known to associate with E2 (Shimura *et al*, 2000), we also examined the effect of 14-3-3η on the ability of parkin to recruit E2. For this purpose, we coexpressed HA-parkin with FL-UbcH7 or FL-Ubc7, both of which are known

to bind to parkin (Shimura *et al* 2000; Imai *et al*, 2001). Almost the same amounts of UbcH7 (Figure 4A) and Ubc7 (Figure 4B) were detected in the anti-parkin immunoprecipitants irrespective of cotransfection with Myc-14-3-3η. These findings indicate that 14-3-3η does not influence the recruitment of E2, that is, UbcH7 or Ubc7, to parkin.

α-Synuclein abrogates 14-3-3η-related parkin inactivation

Based on the above findings, we next examined the mechanism that regulates the 14-3-3η–parkin binding. As α-SN partly has a high homology to 14-3-3 isoforms (Ostrerova *et al*, 1999), we tested the effects of α-SN on the 14-3-3η-induced suppression of parkin. By cotransfection experiments in HEK293 cells, parkin again ubiquitylated synphilin-1, and 14-3-3η inhibited the parkin-mediated ubiquitylation (Figure 5A). Coexpression of α-SN resulted in the recovery of ubiquitylation of synphilin-1 and the association of synphilin-1 with parkin, suggesting that α-SN abrogates the 14-3-3η-induced suppression of parkin (Figure 5A, top panel). Importantly, the familial PD-related mutants of α-SN(A30P) (Kruger *et al*, 1998) and α-SN(A53T) (Polymeropoulos *et al*, 1997) could not abrogate the inhibitory role of 14-3-3η. Similar results were observed by detection of self-ubiquitylation activity of parkin (Figure 5A, second panel).

We then tested whether α-SN can release the binding of Myc-14-3-3η from parkin in cotransfection experiment. As shown in Figure 5B (top panel), FL-parkin was self-ubiquitylated in the absence of 14-3-3η. Coexpression of 14-3-3η inhibited the self-ubiquitylation of parkin, and this was accompanied by the binding of 14-3-3η to FL-parkin. Coexpression of α-SN abrogated the binding of 14-3-3η to parkin and resulted in the recovery of self-ubiquitylation of parkin. These effects were not seen by coexpression of α-SN(A30P) and α-SN(A53T) (Figure 5B, top panel). In addition, while the 14-3-3η–parkin interaction was considerably reduced by α-SN, it was not reduced by α-SN(A30P) or α-SN(A53T) (Figure 5B, bottom panel). Taken together, α-SN, but not α-SN(A30P) or α-SN(A53T), binds strongly to 14-3-3η and thereby releases parkin from the parkin–14-3-3η complex.

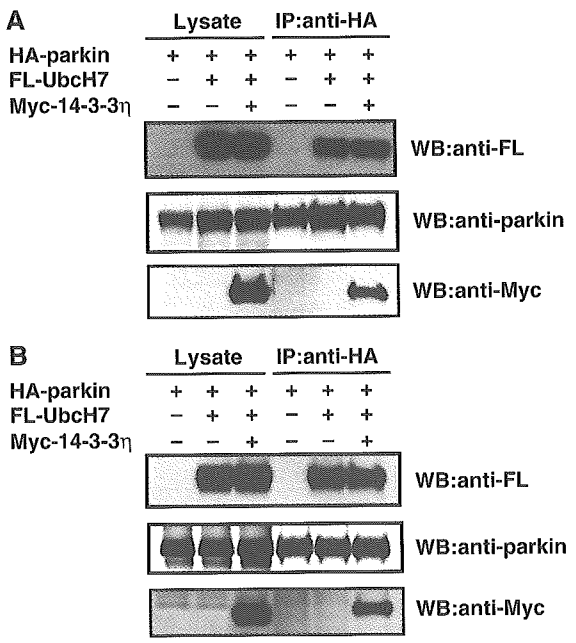

Figure 4 Effect of 14-3-3η on the recruitment of E2 (UbcH7 or Ubc7) to parkin. (**A**) HA-parkin (3 μg), FL-UbcH7 (3 μg), or Myc-14-3-3η (6 μg) plasmids were transfected for 48 h into HEK293 cells at the indicated combinations. After immunoprecipitation with anti-HA antibody, Western blotting was performed using antibodies against FL, Myc, and parkin. (**B**) The experiment was conducted as in (A), except that FL-Ubc7 was used instead of FL-UbcH7.

We also tested the interaction of Myc-14-3-3η with FL-α-SN, FL-α-SN(A30P), and FL-α-SN(A53T). Myc-14-3-3η interacted only with FL-α-SN, but not α-SN(A30P) nor α-SN(A53T) (Figure 5C, upper-top panel), suggesting that α-SN relieves parkin activity from binding to 14-3-3η. The 14-3-3η/α-SN interaction was not affected by parkin (Figure 5C, upper-top panel), and parkin was not associated with α-SN (Figure 5C, upper-second panel). Interestingly, FL-α-SN did not interact with Myc-14-3-3σ, β, and ζ in the same experiment (Figure 5C, lower panel). These results further strengthen the notion that α-SN specifically activates parkin through binding 14-3-3η.

We then investigated whether the interaction of 14-3-3η and parkin is direct or indirect by using purified recombinant His-parkin and GST-14-3-3η. GST or GST-14-3-3η was mixed with His-parkin, and pulled down by glutathione beads. His-parkin bound to GST-14-3-3η, but not GST (Figure 5D, left panel), indicating that parkin directly interacts with 14-3-3η. On the other hand, a similar *in vitro* binding assay showed that GST-14-3-3η did not interact with recombinant α-SN (Figure 5D, right panel), suggesting that certain modification(s) of α-SN may be required for the interaction of 14-3-3η.

Subsequently, we measured the binding affinities of parkin and α-SN for 14-3-3η by the surface plasmon resonance (SPR) method. As shown in Figure 5E, parkin bound 14-3-3η with a considerably strong affinity ($K_d = 4.2$ nM, upper), whereas the affinity of α-SN for 14-3-3η was much lower than that of parkin ($K_d = 1.1$ μM, lower). These results are consistent with those of the immunoprecipitation/Western analysis using recombinant proteins (Figure 5D).

Finally, we examined whether 14-3-3η bound to parkin can be released by α-SN. To test this, we first mixed the lysates coexpressing FL-parkin and Myc-14-3-3η of HEK293 cells with those expressing α-SN. Then the mixtures were incubated under three different conditions, as indicated in the upper panel of Figure 5F. Next, the lysates were immunoprecipitated with anti-FL antibody, and followed by Western blotting with anti-Myc and anti-parkin antibodies. As shown in Figure 5F (upper panel), the amount of 14-3-3η bound to parkin was significantly lower in all incubation conditions, when the cell lysates that simultaneously expressed both parkin and 14-3-3η were incubated with α-SN-expressing lysates. Incubation for 1 h at 37°C reduced the amount of 14-3-3η bound to parkin in proportion to the added amount of α-SN-expressing cell lysate (Figure 5F, lower panel). Intriguingly, the α-SN(A30P) and α-SN(A53T) mutants had no effect on the release of 14-3-3η, unlike wild-type (WT) α-SN (Figure 5F, lower panel). These observations strongly indicate that α-SN, but not α-SN(A30P) or α-SN(A53T), can capture and release 14-3-3η from the parkin–14-3-3η complex, which supports our notion that the negative regulation of parkin activity by 14-3-3η is relieved by α-SN (Figure 5A and B).

Parkin, 14-3-3η, and α-SN levels in the substantia nigra of PD

Finally, we analyzed the levels of parkin, 14-3-3η, and α-SN in the substantia nigra of the midbrain from patients with sporadic PD. Western blotting revealed no significant differences in parkin, 14-3-3η, and actin in the substantia nigra between control (patients without PD) and PD patients, whereas α-SN was significantly increased in the substantia nigra of PD patients (Figure 6A, upper panel). As parkin did not interact physically with α-SN in our immunoprecipitation analysis (Figure 5C; data not shown), we then examined the interactions of 14-3-3η with parkin or α-SN by measuring

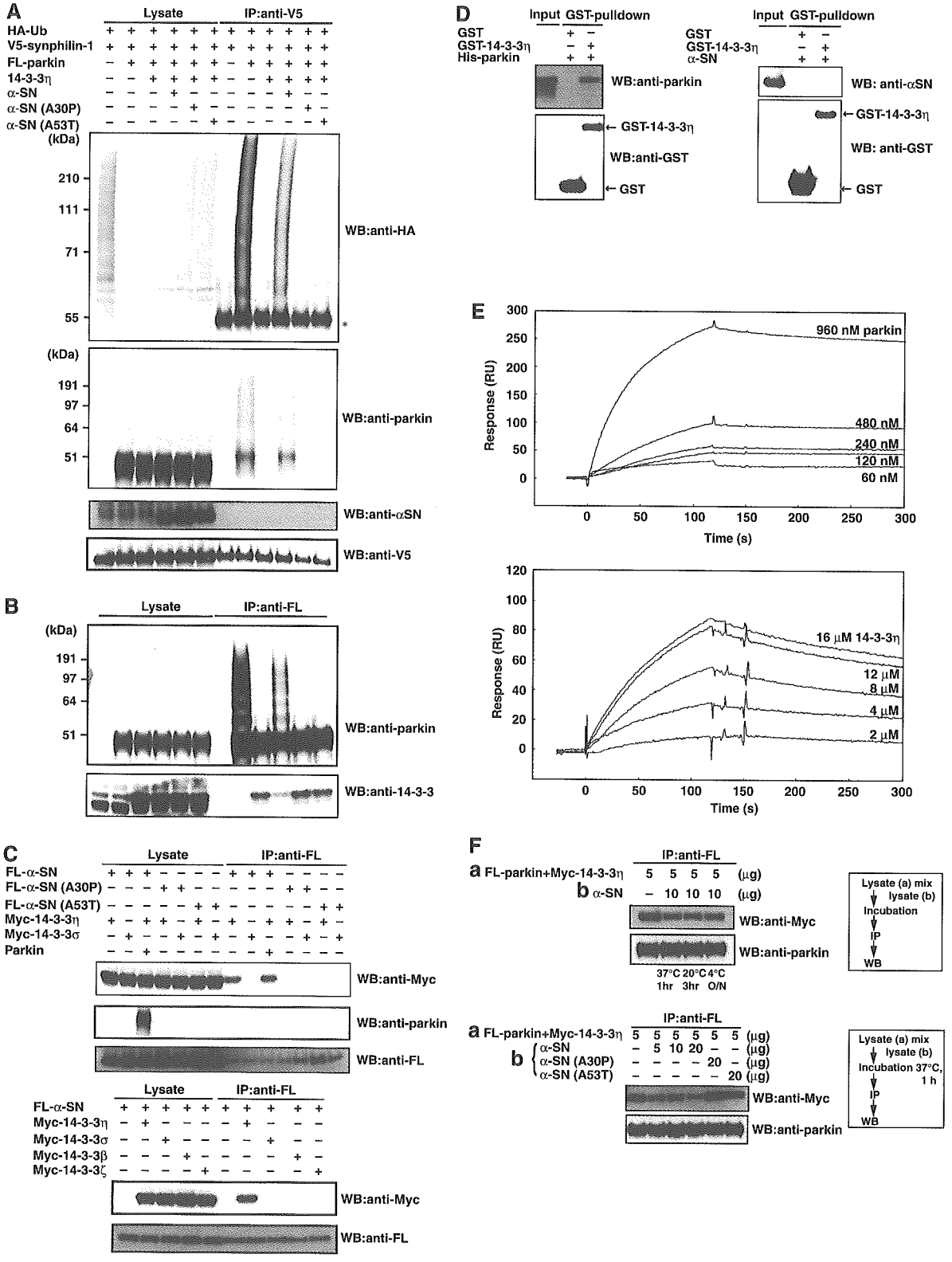

these proteins in the anti-14-3-3η immunoprecipitant. Whereas the levels of parkin associated with 14-3-3η from PD appeared to be decreased relative to the control, the levels of α-SN that interacted with 14-3-3η were clearly increased in patients with PD (Figure 6A, lower panel). Thus, it is suggested that the elevated levels of α-SN are associated with its interaction with 14-3-3η and the activity of parkin may be aberrantly regulated in the substantia nigra of sporadic PD.

Discussion

The major finding of the present study was the identification of 14-3-3η as a novel regulator of parkin. First, parkin was in a complex with 14-3-3η, but not β, γ, ε, or τ isoforms, in the mouse brain (Figure 1). 14-3-3η could bind primarily to the linker region of parkin, but not with the ARJP-causing missense mutant parkin (K161N), which has a mutation in the

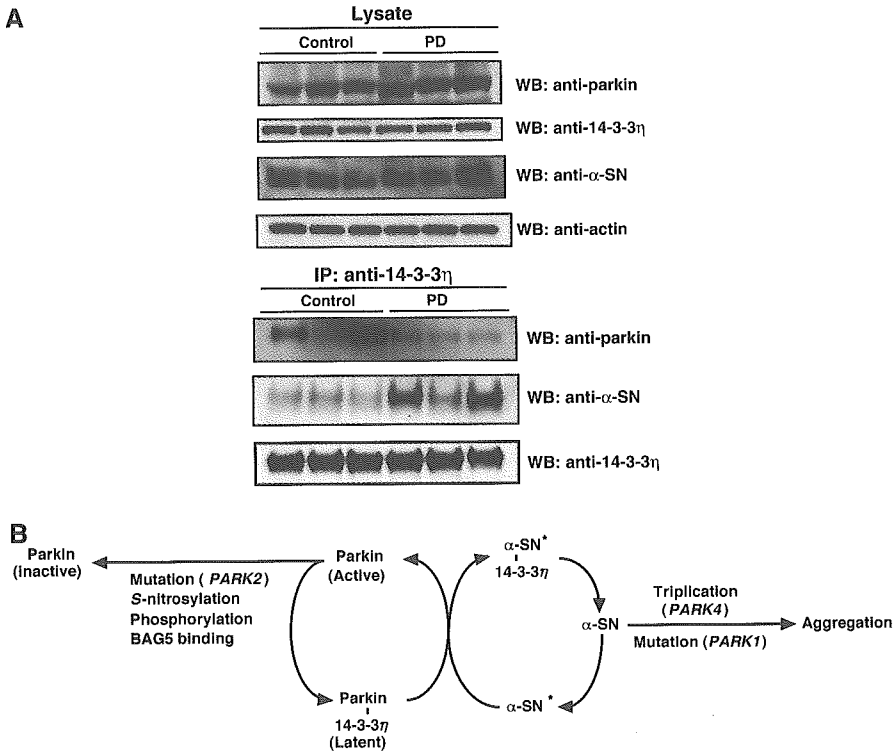

Figure 6 (**A**) Levels of parkin, 14-3-3η, and α-SN in the substantia nigra of PD. Brain of a representative patient with PD (upper panel). Samples (30 μg) of the crude extract of the brains (substantia nigra) of control (patients without PD) and PD patients were subjected to SDS–PAGE, following Western blotting against antibodies against parkin, 14-3-3η, α-SN, and actin. Physical interaction between 14-3-3η and parkin or α-SN (lower panel). After the same samples used in the upper panel were immunoprecipitated with anti-14-3-3η, Western blotting was carried out using antibodies against parkin, α-SN, and 14-3-3η. (**B**) A schematic diagram showing the pathways involved in the regulation of parkin activity by 14-3-3η and α-SN. α-SN, α-synuclein; α-SN*, modified form of α-SN. Note that whether parkin is phosphorylated to bind to 14-3-3η remains unknown at present. See text for details.

Figure 5 Effects of α-SN on 14-3-3η-induced suppression of parkin E3 activity and interaction between 14-3-3η and α-SN in HEK293 cells. (**A**) Ubiquitylation of synphilin-1. Transfection was conducted at various combinations, as in Figure 3C, except for cotransfection of 4 μg of α-SN, α-SN(A30P), and α-SN(A53T). After immunoprecipitation with anti-V5 antibody, Western blotting was carried out with antibodies against HA, parkin and α-SN, and V5. Asterisk denotes an IgG heavy chain. (**B**) Autoubiquitylation of parkin. Transfection was performed as in (A). After immunoprecipitation with anti-FL antibody, Western blotting was carried out with antibodies against parkin and 14-3-3. (**C**) Interaction of 14-3-3η and α-SN with or without parkin. Various expression vectors at the indicated combinations were transfected. Immunoprecipitation was conducted by anti-FL antibody and the resulting immunoprecipitates were used for Western blotting with antibodies against Myc, parkin, and FL. (**D**) Physical interaction between 14-3-3η and parkin (left panel) or α-SN (right panel) in recombinant proteins. After recombinant His-tagged parkin produced from baculovirus-infected HiFive insect cells (3 μg) or GST-α-SN expressed in *E. coli* whose GST moiety was removed by PreScission Protease digestion prior to use (3 μg) was incubated for 1 h at 32°C with 3 μg of GST or GST-tagged 14-3-3η expressed in *E. coli*, glutathione-Sepharose was added and the incubation vessels were slowly rotated for 3 h at 4°C. The washed Sepharose resin was eluted with 50 μl of 50 mM Tris–HCl (pH 8.0) buffer containing 10 mM reduced glutathione, and aliquots (15 μl) were analyzed by Western blotting with antibodies against parkin (left-top panel), α-SN (right-top panel), and GST (bottom panel). Input: 500 ng of parkin or α-SN. (**E**) SPR analyses of parkin and α-SN binding to 14-3-3η. Upper: subtracted sensorgrams of interaction between a subset of parkin concentrations and immobilized 14-3-3η. Lower: subtracted sensorgrams of interaction between a subset of 14-3-3η concentrations and immobilized α-SN. (**F**) Sequestration of 14-3-3η by α-SN from the parkin–14-3-3η complex. Various expression vectors were transfected as indicated. Upper panel: 5 μg of the lysate-(a) from cells co-expressing FL-parkin and Myc-14-3-3η were mixed with 10 μg of cellular lysate-(b) expressing α-SN. The mixtures were incubated under various conditions; that is, 37°C for 1 h, 20°C for 3 h, or overnight at 4°C (O/N), then immunoprecipitation by anti-FL antibody was conducted, followed by Western blotting with antibodies against Myc (14-3-3η) and parkin. Lower panel: the experiments were conducted as for the top panel, except that incubation was carried out at 37°C for 1 h using α-SN-, α-SN(A30P)-, or α-SN (A53T)-expressing lysates as indicated. The experimental protocol is shown in the flow charts on the right.

linker region (Figure 2). Second, the binding of 14-3-3η to parkin was associated with suppression of the ubiquitin-ligase activity, suggesting that certain parkin bound to 14-3-3η is present at a latent status in the brain (Figure 3). Third, overexpression of α-SN abrogated the 14-3-3η-induced suppression of parkin activity, indicating that α-SN relieves the negative regulation of parkin by 14-3-3η (Figure 5A and B). Intriguingly, PD-causing A30P and A53T mutations of α-SN could not bind 14-3-3η and failed to activate parkin. These results indicate that 14-3-3η is a regulator that functionally links parkin and α-SN, as illustrated in Figure 6B.

It is of particular note that we report unusual isoform specificity for 14-3-3η to interact with parkin among all 14-3-3 species examined. However, the possibility that the other species are also involved in the interaction by forming a heterodimer with 14-3-3η cannot be excluded *in vivo*, because 14-3-3 bands immunoprecipitated by anti-parkin antibody from the brain extracts showed doublet with one weak signal for Western blotting (Figure 1A). Nevertheless, herein we address that recombinant parkin could directly bind to 14-3-3η (Figure 5D, left panel), with considerably high affinity (K_d = approximately 4 nM) (Figure 5E) and that the 14-3-3η homodimer is a negative factor for autoubiquitylating activity of parkin *in vitro* (Figure 3A).

It is known that the 14-3-3 family proteins interact with the majority, but not all, proteins after their phosphorylation (Aitken *et al*, 2002; Bridges and Moorhead, 2004; Mackintosh, 2004). Indeed, parkin contains the RKDSPP sequence in the linker region that resembles the typical binding motifs with a potential phosphorylation residue for 14-3-3 proteins (Yaffe *et al*, 1997; Mackintosh, 2004). It is also known that parkin has several possible phosphorylation sites, and recent studies showed that parkin is phosphorylated *in vitro* (Yamamoto *et al*, 2004), although there is no direct evidence demonstrating phosphorylation of parkin *in vivo* to date. However, it remains elusive whether or not phosphorylation of parkin is responsible for its specific binding to 14-3-3η, because known potential phosphorylation motifs are capable of associating with many 14-3-3 species in general. The specificities of 14-3-3: client–protein interactions do not result from different specificities for the phosphopeptide-binding motifs, but probably arises from contacts made on the variable surface of 14-3-3 outside the binding cleft, as discussed previously by Yaffe *et al* (1997). In this regard, some reports showed functional specificities of 14-3-3 isoforms (Aitken, 2002; Aitken *et al*, 2002; Roberts and de Bruxelles, 2002), and indeed several enzymes retain several nonphosphorylated binding motifs for 14-3-3s (Hallberg, 2002; Sribar *et al*, 2003), though parkin lacks such 14-3-3-interacting sequences. Thus, parkin, in particular its linker region, may have a new binding motif(s) for 14-3-3η, but the interacting motif(s) remains to be identified. If 14-3-3η binds to parkin through two sites as a dimmer, it is plausible that the phosphorylation of parkin is involved in their interactions at least in part.

With regard to the mechanistic action of 14-3-3η, it may suppress parkin activity by preventing access of the substrate, because the binding of synphilin-1 (used here as a model substrate to parkin) was inhibited by 14-3-3η (Figure 3C). Accumulating evidence suggests that parkin can bind various targets by the UBL domain or the RING box, in particular the RING 1 domain (Dawson and Dawson, 2003). Accordingly, 14-3-3η may have function(s) other than suppressing the access of the substrate to parkin. Indeed, 14-3-3η strongly inhibits substrate-independent self-ubiquitylation of parkin, indicating blockage of the intrinsic E3 activity. It was also anticipated that 14-3-3η hinders the recruitment of E2 to parkin. However, this was not the case, because 14-3-3η had no effect on the binding of UbcH7 and Ubc7 to parkin (Figure 4). Thus, while the mechanism of 14-3-3η-induced suppression of parkin activity remains to be identified, it is possible that it involves preventing the positioning of the ubiquitin-charged E2 toward the target Lys residue by steric hindrance due to the association of 14-3-3η to parkin.

It is worth noting that parkin does not interact with α-SN directly, because we could not demonstrate the physical binding of parkin to α-SN *in vivo* and *in vitro* (data not shown; see also Dawson and Dawson, 2003). Nevertheless, we found that the negative regulation of parkin by 14-3-3η was relieved by α-SN, which could bind tightly to 14-3-3η *in vivo* (Figure 5A–C). In this regard, it is of note that the amounts of 14-3-3η bound to parkin were decreased when the lysates of cells coexpressing parkin and 14-3-3η were incubated with those expressing WT α-SN, but not PD-related α-SN(A30P) or α-SN(A53T) mutants *in vitro* (Figure 5F). These results clearly indicate that 14-3-3η bound to parkin is sequestered by α-SN, but not competition by α-SN toward the binding of 14-3-3η to parkin. Unlike the association between parkin and 14-3-3η, there is little or no interaction between α-SN and 14-3-3η *in vitro*, as recombinant α-SN did not bind to 14-3-3η (Figure 5D, right panel, and E). Thus, it is plausible that certain modification(s) of α-SN is required for its association to 14-3-3η in mammalian cells (see our model in Figure 6B). Judging from the characteristic properties of 14-3-3 family proteins capable of binding many phosphorylated proteins (Yaffe *et al*, 1997), certain phosphorylation(s) of α-SN seems quite possible for the interaction with 14-3-3η. Indeed, there are several reports regarding phosphorylation of α-SN (Fujiwara *et al*, 2002; Hirai *et al*, 2004). Although previous studies clearly demonstrated that α-SN deposited in synucleinopathy brains is extensively phosphorylated at Ser-129 (Fujiwara *et al*, 2002; Hirai *et al*, 2004), this is probably not the case in our study, because the chemically synthesized peptide phosphorylated at Ser-129 of α-SN did not bind to the 14-3-3η (our unpublished results). However, the possibility that α-SN is phosphorylated at other site(s) cannot be exclusively ruled out. Alternatively, one cannot exclude a possible, though yet unknown, modification(s) of α-SN other than phosphorylation as a mechanism responsible for the increased affinity toward 14-3-3η. In this regard, α-SN is structurally related to 14-3-3 family proteins (Ostrerova *et al*, 1999), but it is unknown whether the homologous region is involved in the physical interaction with α-SN. Further studies are required to clarify the mode of α-SN modification.

In the present study, we found reciprocal regulation of parkin activity by α-SN and 14-3-3η, whose tripartite control could enhance our understanding of the pathogenesis of PD. As illustrated in Figure 6B, to date there are several reports on the post-translational modification of parkin. Recent findings indicate that the ubiquitin E3 ligase activity of parkin is modified by nitric oxide (NO). Namely, parkin is *S*-nitrosylated in PD patients and an *in vivo* mouse model of PD, and *S*-nitrosylation shows inhibition of the E3 activity of

parkin (Chung *et al*, 2004; Kahle and Haass, 2004; Yao *et al*, 2004), which could contribute to the degenerative process in PD by impairing the ubiquitylation of parkin substrates. Moreover, Kalia *et al* (2004) showed that the bcl-2-associated athanogene 5 (BAG5) enhanced the death of dopaminergic neurons in an *in vivo* model of PD by inhibiting the E3 ligase activity of parkin. In addition, recent studies reported that phosphorylation of parkin causes a small but significant reduction of parkin auto-ubiquitylating activity (Yamamoto *et al*, 2004). More recently, it was reported that Nrdp1/FLRF RING-finger E3 ligase binds and ubiquitylates parkin, resulting in reduction of parkin activity, implying its involvement in the pathogenesis of PD (Zhong *et al*, 2005). Considered together, these results indicate that the apparent loss of parkin E3 ubiquitin ligase activity associated with the pathogenesis of PD (see the model displayed in Figure 6B) is in agreement with the ARJP-linked mutations that lead to loss of function of parkin, and that the functional loss of parkin activity is linked to the death of dopaminergic neurons. In addition, we reported herein the imbalance of tripartite interactions among parkin, 14-3-3η, and α-SN levels in the substantia nigra of sporadic PD, but it is still not clear how these alterations influence parkin activity in neural cells. Thus, parkin is an E3 ubiquitin ligase involved in the ubiquitylation of proteins, irrespective of its involvement of K48- or K63-linked ubiquitylation (Doss-Pepe *et al*, 2005; Lim *et al*, 2005), that are important in the survival of dopaminergic neurons in PD.

In the present study, we found that parkin E3 activity is regulated positively and negatively by α-SN and 14-3-3η, respectively, suggesting that derangements of this regulation may be responsible for ARJP. For instance, the activated parkin free from 14-3-3η may be labile, and thus sensitive to other stresses, such as *S*-nitrosylation, and inactivated secondarily in PD. This situation resembles the effect of *S*-nitrosylation, in which nitrosative stress leads to *S*-nitrosylation of WT parkin, which leads initially to a marked increase followed by a decrease in the E3 ligase–ubiquitin–proteasome degradative pathway (Yao *et al*, 2004). The initial increase in the activity of parkin's E3 ubiquitin ligase leads to autoubiquitylation of parkin and subsequent inhibition of its activity, which would impair ubiquitylation and clearance of parkin substrates. In turn, 14-3-3η may protect against impairment of parkin induced by various environmental stresses, including *S*-nitrosylation. It is also noteworthy that, although 14-3-3η acts as a negative regulator of parkin, it may play a positive role in maintaining a large pool of parkin by preventing its self-ubiquitylation in the brain. Finally, we assume that gradual reduction of parkin activity may be associated with the development of ARJP as well as sporadic PD.

Current evidence suggests that α-SN increases in response to various stresses (Sherer *et al*, 2002; Gomez-Santos *et al*, 2003). This finding is compatible with the results of recent studies that dopamine-dependent neurotoxicity (Tabrizi *et al*, 2000; Zhou *et al*, 2000; Junn and Mouradian, 2002) is mediated by the formation of protein complexes that contain α-SN and 14-3-3, which are selectively increased in the substantia nigra in PD (Xu *et al*, 2002). Further studies are needed to determine the levels of parkin, 14-3-3η, α-SN, and parkin and α-SN-14-3-3η complexes in the substantia nigra of the midbrain of patients with sporadic PD.

Here we suggest that α-SN and parkin function through the same pathway. Indeed, both proteins, if not all, are associated with presynaptic vesicles (Dawson and Dawson, 2003). So far, however, the physiological role of α-SN is largely unknown, though various roles including its involvement in synaptic plasticity have been suggested (Liu *et al*, 2004). We here provided the first evidence that α-SN acts as a positive regulator of parkin E3 activity. It is worth noting that disease-causing mutations of α-SN(A30P) and α-SN(A53T) could not activate the latent parkin–14-3-3η complex, and thus, these mutations may accelerate the development of PD by failing to activate parkin. Our results identified a functional link between these two familial PD-gene products, thus highlighting the existence of a novel regulatory mechanism that could help us further understand the pathogenesis of ARJP as well as sporadic PD. However, it must be stressed here that α-SN is the causative gene product of familial PD. It is noteworthy that α-SN is an aggregation-prone protein due to its natively unfolded protein nature. It is of note that the locus of *PARK4* is triplication of the *α-SN* gene (*PARK1*) (Singleton *et al*, 2003), indicating that overexpression of α-SN itself is toxic and induces dopaminergic neuronal death. Indeed, α-SN tends to self-aggregate, and this tendency, which is augmented in the α-SN(A30P) and α-SN(A53T) mutants (Conway *et al*, 2000) (see our model in Figure 6B), causes autosomal dominant PD (Narhi *et al*, 1999). Both WT and mutant α-SN form amyloid fibrils akin to those seen in LBs, as well as nonfibrillary oligomers termed protofibrils (Dawson and Dawson, 2003; Bossy-Wetzel *et al*, 2004). However, whether aggregation and fibrillary formation of α-SN- and PD-linked mutants play a role in neuronal dysfunction and death of neurons in PD are a matter of fierce debate. At this point of view, we emphasize that the feature of α-SN as an aggregation-prone protein is probably not linked directly to its role as a potent activator of parkin E3 in the pathogenesis of PD. Even if these two unique properties of α-SN account for the development of PD independently or synergistically, however, it is clear that their mechanistic actions differ as illustrated in Figure 6B.

Materials and methods

Immunological analysis

For immunoprecipitation analysis of endogenous proteins in the brains of adult mouse and human, these brains were homogenized in three volumes of ice-cold lysis buffer (20 mM HEPES (pH 7.9) buffer containing 0.2% NP-40, 1 mM dithiothreitol (DTT) and protease inhibitor cocktail (Sigma, Chemical Co., St Louis, MO)). The tissue homogenate was centrifuged at 20 000 *g* at 4°C for 20 min. The supernatant (2 mg protein) was used for immunoprecipitation with one of the following antibodies: anti-polyclonal parkin (Cell Signaling Technology, Beverly, MA) and anti-14-3-3η antibodies (Immuno-Biological Lab. Co., Gunma) or control IgG (700 ng). The resulting immunoprecipitates were resolved in 30 μl of the sodium dodecyl sulfate–polyacrylamide gel electrophoresis (SDS–PAGE) sample buffer, and one-third of the samples (10 μl) were subjected to SDS–PAGE, followed by Western blotting with anti-14-3-3 (Santa Cruz Biotechnology, Santa Cruz, CA), anti-14-3-3β, 14-3-3γ, 14-3-3ε, 14-3-3η, and 14-3-3τ (Immuno-Biological Lab. Co., Ltd, Japan) and anti-monoclonal parkin (1A1) antibodies (Shimura *et al*, 1999). In all, 10 μg of the supernatant (lysate) was used as input (1.5%).

For immunoprecipitation analysis of the cell culture system, HEK293 cells were transfected with the respective plasmids. After 48 h, the cells were washed with ice-cold PBS (in mM, 10 Na_2PO_4, 2 KH_2PO_4, 137 NaCl, and 2.7 KCl), pH 7.4, and harvested in the lysis buffer (600 μl). The lysate was then rotated at 4°C for 1 h, followed by centrifugation at 20 000 *g* for 10 min. The supernatant (200 μl) was then combined with 50 μl protein G-Sepharose (Amersham Life